FIRAT UNIVERSITY

GRADUATE SCHOOL OF NATURAL AND APPLIED SCIENCES

TÜRKİYE

SYNTHESIS AND CHARACTERIZATION OF STRONTIUM-BASED HYDROXYAPATITES DOPED WITH ERBIUM

Bahroz Kareem MAHMOOD

Master's Thesis

DEPARTMENT OF PHYSICS

Division of Solid State Physics

20 JULY 2020

FIRAT UNIVERSITY
GRADUATE SCHOOL OF NATURAL AND APPLIED SCIENCES
TÜRKİYE

Department of Physics

Master's Thesis

SYNTHESIS AND CHARACTERIZATION OF STRONTIUM-BASED HYDROXYAPATITES DOPED WITH ERBIUM

Author
Bahroz Kareem MAHMOOD

Supervisor
Assoc. Prof. Dr. Ömer KAYĞILI

20 JULY 2020

ELAZIG

FIRAT UNIVERSITY

GRADUATE SCHOOL OF NATURAL AND APPLIED SCIENCES

TÜRKİYE

Department of Physics

Master's Thesis

Title:	Synthesis and Characterization of Strontium-Based Hydroxyapatites Doped with Erbium
Author:	Bahroz Kareem MAHMOOD
Submission Date:	23 June 2020
Defense Date:	20 July 2020

THESIS APPROVAL

This thesis, which was prepared according to the thesis writing rules of the Graduate School of Natural and Applied Sciences, Fırat University, was evaluated by the committee members who have signed the following signatures and was unanimously approved after the defense exam made open to the academic audience.

Signature

Supervisor:	Assoc. Prof. Dr. Ömer KAYĞILI Firat University, Faculty of Science	Approved
Chair:	Prof. Dr. Niyazi BULUT Firat University, Faculty of Science	Approved
Member:	Assist. Prof. Dr. Tankut ATEŞ Malatya Turgut Özal University, Faculty of Engineering	Approved

This thesis was approved by the Administrative Board of the Graduate School on
.... / .... / 20 ....

Signature

Prof. Dr. Soner ÖZGEN
Director of the Graduate School

DECLARATION

I hereby declare that I wrote this Master's Thesis titled " Synthesis and Characterization of Strontium-Based Hydroxyapatites Doped with Erbium" in consistent with the thesis writing guide of the Graduate School of Natural and Applied Sciences, Firat University. I also declare that all information in it is correct, that I acted according to scientific ethics in producing and presenting the findings, cited all the references I used, express all institutions or organizations or persons who supported the thesis financially. I have never used the data and information I provide here in order to get a degree in any way.

20 July 2020

Bahroz Kareem MAHMOOD

PREFACE

The study in bioceramic materials is very important, because currently bioceramics have a great interest in nanotechnology and medical applications. Hydroxyapatite (HAp), is one of the most important calcium orthophosphate bioceramics. Since it is comprising most of the human hard tissues compositions and has great interest in biomedical applications. Due to its excellent properties that required in medical applications. Additionally, HAp have a great future in medical application, due to increase the number of peoples that needs medical implant surgery.

I would like to interpret huge thanks and appreciate to my supervisor Assoc. Prof. Dr. Ömer KAYĞILI, he was always helped and supported me during my study and dissertation. Also, I would thank Prof. Dr. Niyazi BULUT for his help and valuable contributions in preparing this dissertation. Great thanks to my wife and my parents for their supports who abandon their rights for sake my success.

Bahroz Kareem MAHMOOD
ELAZIG, 20 JULY 2020

TABLE OF CONTENTS

ABSTRACT

Synthesis and Characterization of Strontium-Based Hydroxyapatites Doped with Erbium

Bahroz Kareem MAHMOOD

Master's Thesis

FIRAT UNIVERSITY
Graduate School of Natural and Applied Sciences

Department of Physics

20 July 2020,   Page: xi + 38

In this thesis, the main purpose is to study the effects of strontium (Sr) and erbium (Er) dopants on the characteristic properties of hydroxyapatite (HAp). The HAp samples with fixed amount of Sr 0.35 at% and Er with various amounts of 0, 0.35, 0.70, 1.05, and 1.40 at % were synthesized by using wet chemical method.

The samples were characterized by X-ray diffraction (XRD), scanning electron microscopy (SEM), energy dispersive X-ray (EDX), Fourier transform infrared (FTIR) spectroscopy, differential thermal analysis (DTA), as well as *in vitro* biocompatibility analysis. In addition, the density of states (DOS) and band structures were investigated theoretically.

In all samples, single-phase of HAp was detected. For the two different methods, the crystallinity percentage of the samples was estimated to be 89% or more. The crystallite sizes of the samples were computed to be in the range of 29-34 nm for Scherrer method, and 25-42 nm for Williamson-Hall method. DTA investigations revealed that all samples in temperature range from 25 °C to 1000 °C exhibited thermal stability. EDX results indicated that Ca-deficiency has occurred with increase in Er amount. No significant change was observed in the morphology of the samples. Additionally, is was found that the band structures turned to tightening with an increase in Er concentration from the theoretical study results.

Keywords: Strontium, Erbium, Hydroxyapatite, Wet chemical method, X-ray diffraction (XRD), Band structure

ÖZET

Stronsiyum Esaslı Erbiyum Katkılı Hidroksiapatitlerin Sentez ve Karakterizasyonu

Bahroz Kareem MAHMOOD

Yüksek Lisans Tezi

FIRAT ÜNIVERSITESI
Fen Bilimleri Enstitüsü

Fizik Anabilim Dalı
20 July 2020,   Sayfa: xi + 38

Bu tezde asıl amaç, stronsiyum (Sr) ve erbiyum (Er) katkılarının hidroksiapatitin (HAp) karakteristik özellikleri üzerindeki etkilerini incelemektir. Sabit miktarda Sr (at.% 0.35) ve çeşitli miktarlarda (at.% 0, 0,35, 0,70, 1,05 ve 1,40) Er içeren HAp numuneleri yaş kimyasal yöntem kullanılarak sentezlendi.

Numuneler, *in vitro* biyouyumluluk analizinin yanı sıra X-ışını kırınımı (XRD), taramalı elektron mikroskopisi (SEM), enerji dağılımlı X-ışını (EDX), Fourier dönüşümlü kızılötesi (FTIR) spektroskopisi, diferansiyel termal analiz (DTA) edildi. İlave olarak, durum yoğunlukları (DOS) ve bant yapıları teorik olarak incelenmiştir.

Tüm numunelerde, tek fazlı HAp tespit edildi. İki farklı yöntem için, numunelerin kristalleşme yüzdesi % 89 veya daha fazla olarak hesaplandı. Numunelerin kristal boyutlarının Scherrer metodu için 29-34 nm ve Williamson-Hall metodu için 25-42 nm aralığında olduğu hesaplandı. DTA araştırmaları, 25 °C ile 1000 °C arasındaki sıcaklıklarda tüm numunelerin termal kararlılık gösterdiğini ortaya koydu. EDX sonuçları, Er miktarındaki artışla Ca eksikliğinin meydana geldiğini gösterdi. Numunelerin morfolojisinde önemli bir değişiklik gözlenmedi. Ek olarak, teorik çalışma sonuçlarından, bant yapılarının Er konsantrasyonundaki artışla sıkılaşmaya başladığı bulundu.

Anahtar Kelimeler: Stronsiyum; Erbiyum; Hidroksiapatit; Yaş kimyasal yöntem; X-ışını kırınımı (XRD); Bant yapısı

LIST OF FIGURES

LIST OF TABLES

LIST OF SYMBOLS

Symbols

---

a, b and *c* : Lattice parameters

DOS : Density of states

D_{WH} : Crystallite size (calculated from Williamson-Hall equation)

D_S : Crystallite size (calculated from Scherrer equation)

E_g : Band gap energy

u : Anisotropic energy density

V : Volume of the unit cell

$X_C\%$: Crystallinity percentage calculated from general equation

$X_{CL}\%$: Crystallinity percentage calculated from Landi equation

Y : Young's modulus

α, β, γ : Angles

β : Full width at half maximum

ε : Lattice strain

σ : Lattice stress

λ : Wavelength

θ : Diffraction angle

LIST OF ABBREVIATIONS

Abbreviations

ACP : Amorphous calcium phosphate

Al_2O_3 : Alumina

CAP : Calcium phosphate

CSD : Calcium sulfate dihydrate

DTA : Differential thermal analysis

EDX : Energy dispersive X-ray

FTIR : Fourier transform infrared

HCP : Hexagonal close-packet

KBr : Potassium bromide

SEM : Scanning electron microscopy

Sr-HAp : Strontium based hydroxyapatite

XRD : X-ray diffraction

α-TCP : Alpha tricalcium phosphate

β-TCP : Beta tricalcium phosphate

ZrO_2 : Zirconia

1. INTRODUCTION

Since the existence of humans on the earth planet continuously in search to improve life quality and achieve the necessaries. Science is the unique factor of making human life better and easier. As well as, material science is one of the most important branches of science.

Material science is an interdisciplinary area dealing with the acknowledging and applying the properties of materials, researchers are studying the relations between materials structures, characteristics, preparation methods, and application functionalities. It includes different groups of materials, one of the most essential and applicable materials is a biomaterials [1].

Biomaterials are those materials that can be natural or synthetic which designed to replace damaged tissue or organs in contact with a biological system. Biomaterial's history began with gold and ivory. When before the 20th century these materials were used by Egyptians and Romans. The main difference between biomaterials and other materials is its biocompatibility in the human biological system. Therefore, it makes a very interest material in the medical field and used in various medical applications [2, 3]. Over the last fifty years, synthetic biomaterials were used instead of natural biomaterials and became an exciting field and very quick growth. Since they provide better performance and reproducibility in medical devices. This move forward makes the increase in the use of biomaterials. Wherever, caused to save or refine the huge number of people's lives by the devices such as hip joint, heart valve and bone implant [4, 5]. The use of biomaterials applications increases daily, because of the diseases and accidents which humans are facing daily. Moreover, due to the increase in population, there are more patient needs orthopedic surgery[6]. Furthermore, these studies belong to using biomaterials in bone regeneration, cardiovascular repair, and regeneration [7, 8]. The synthetic biomaterials have been classified into distinct sorts by regarding their, chemical, structural and biological characteristics with various degrees of bioactivity such as metal, polymer, composite, and ceramic biomaterials [9]. Metallic materials are usually employed for load-bearing applications such as replacement of joints, screws, and bone plates. Polymer biomaterials are usually employed to the medical applications that non-load-bear like a facial prostheses, cardiovascular prostheses, drug delivery, and in cartilage. Also, the advanced polymers which exist in different forms (i.e.: film, liquid, and gel) that are used as fillers, anti-adhesion material, and coatings. Additionally, the composite materials are relatively recent class of biomaterials that might be natural or synthetic or mix of both and has been used widely for a specific orthopedic surgery [10, 11].

Ceramic biomaterials are one of the biomaterials types, and they are extremely biocompatible, brittle, and exhibit resistance to corrosion. Due to their brittleness, they are used in bone substitution and bone regeneration. Furthermore, they have a low resistance to the load-bearing applications, for this reason, they mostly using as a coating on the strong substrates in

tissue implants. The bioceramic materials have a great interest in biomedical applications, due to exhibits the outstanding properties that required in orthopedics [10].

The one of the most imperative ceramics is Hydroxyapatite (HAp), because it is mostly identical to the bones and teeth inorganic component. Additionally, it exhibits some fundamental important properties. This resulted to use widely in biomedical applications, such as its graet biocompatibility, thermal stability, very high bioactivity, and non-toxicity. Hydroxyapatite applications in orthopedic are restricted due to it is weak mechanical properties. Beside it, hydroxyapatite has the ability to substitute its ions with various foreign ions that may lead to achieving better biocompatibility, mechanical properties and microstructure [12, 13]. A lot of techniques have been developed to synthesize HAp nanoparticle including sol-gel, hydrothermal, mechanochemical, combustion, spray pyrolysis and wet chemical. In addition, the hydroxyapatite characteristics can be changing or controlling by the synthesis methods [14]. The wet chemical method has been elaborated to synthesize HAp nanoparticles with the lowest impurity and most homogenous and its widely used by scholars as a result of its low-cost, simplicity, and low-temperature reaction [15]. Strontium (Sr) is a vital component in the human body in a small quantity, strontium work like calcium because it also prevents the resorption of bone. Additionally, prevent bone loss and improve bone healing, bone strength and micro architecture [14, 16]. Currently, one of the most interest materials in biotechnology is the rare earth elements. Erbium (Er), is one of the rare earth elements, it has been revealed that (Er) exist in rib bones and kidneys. Furthermore, adding (Er) as a dopant to hydroxyapatite possible to improve hydroxyapatite biological properties [17]. Additionally, erbium is essential to doping into other material, to rising luminescence and biocompatibility property, since erbium exhibit good light emission and biocompatibility. As a result, of these properties this element used in optical engineering and in the bone healing process [18].

Particularly, we did not find ever any studies in which both strontium (Sr) and erbium (Er) used as a co-dopant into HAp structure. In this thesis framework; Sr-based HAp samples containing various amounts of (Er) were prepared by wet chemical method and the impact of (Er) addition on the crystal structure, morphology, thermal properties, and biocompatibility were experimentally investigated. As well as, the density of states and band structures was theoretically investigated.

1.1. Biomaterials

Biomaterials can be well-defined as the material that engineered to lonely or as a part of complex medical devices, used to take place diseased or damaged tissue in contact with the biological system [19]. Biomaterials use in the human body is date back to a long time ago. Etruscan civilization around 2,600 years ago, used gold wire to replace the upper incisor with a cow tooth to the adjacent teeth [20]. During an increase, the human knowledge metallic materials came into prosthetic operation. In 1849 many successful operations performed with the metal sutures. In 1924 different materials have been tested in a dog such as iron, and steel, as noted corroded in short time duration, caused to resorption in the surround of bone. Magnesium, nickel, copper, and aluminum alloy, as well as caused to discolor of tissue surrounds. Silver, aluminum, gold, and lead are allowed, but their mechanical properties insufficient. In this stage there was no enough knowledge about biocompatibility, using this metal was continuous for more years. In 1929 Vitallium alloy was used successfully in dentistry. Furthermore, titanium and alloy have been discussed in 1947 as a suitable material for medical implants [4, 5, 21, 22].

In the middle of the last century, the biomaterial encountered to a new stage, two forms of ceramic, alumina and zirconia have been studied successfully as a synthetic implant without making any problem to the living system. Whenever these materials are extremely inert in terms of could not make the bond with the host tissue. As well as, these problems were treated after coming across of bioactive ceramics, such as bioactive glass and hydroxyapatite (HAp) [23]. The main difference between biomaterials and the other material was being used before is the biocompatibility, in terms of biomaterials are maintain as itself, and did not lead to harm to the host tissue or its environment. Biomaterial science is a multidisciplinary science because it makes a combination, physics, chemistry, engineering, and medicine together. Biomaterial has a great future since it can solve more health problems in a different part of the human body [24, 25]. Biomaterials include different materials regarding their physical, chemical, mechanical, and biological properties that can be used in certain orthopedics. The application of biomaterials in various part of the human body is shown in Figure 1.1.
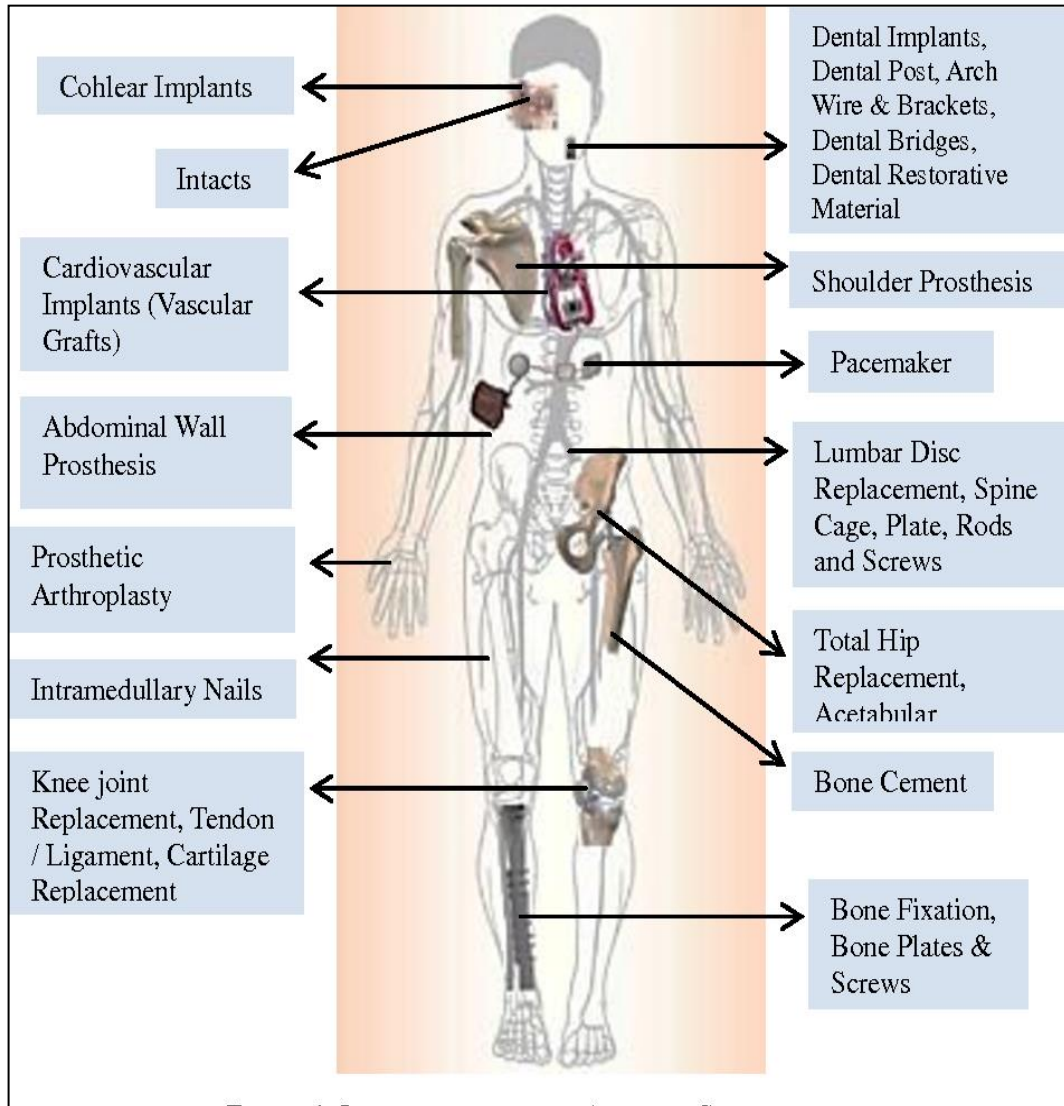
Figure 1.1. Biomaterials application in different tissues of the human body [26].

1.2. Biocompatibility

Biocompatibility is consisting of the necessary properties that any biomaterial needs to display when seated in the living tissues of the biological system. It shows the capacity of the material to be present together in interaction with the tissues without leading harmful impacts that could settlement with health and the function of the tissues [20]. The most important characteristic in a medical implant is biocompatibility, in the term of, the exposed material to the lives tissue must not lead to a harmful reaction with host tissue or its surroundings and the health of the recipient. Biomaterials should be non-mutagenic, non-allergenic, non-carcinogenic, and non-toxic. Furthermore, since toxic materials might be leading to membrane injury and damage the metabolic pursuit impacts within the cell. As a result, these occasions might eventually lead to

4

cell decomposition and death [27, 28]. For these reasons, selecting the metallic materials for the implant should be taking attention to corrosion because the living system of the human body is an extremely corrosive medium for metallic materials. Since the human biological system encompasses different ions, as a result, the degradation of oxygen and hydroxyl will occur during chemical reaction cause to corrode the metal, the compound produced throughout the corrosion process will react with live tissue cause implant failing and harm the patient health [29]. Furthermore, any biomaterial has an aspect of biocompatibility and the others may not have, for this reason in some application two or more using together as well as in coating [30]. In the term of biocompatibility, any biomaterial used in medicine must exhibit biosafety and bio functionality within the host tissue. Biocompatibility, differ from recipient to recipient due to their situations and the procedures used to supervise the biomaterial to the recipient [31]. Therefore, before using any material in medical applications must be studied it is biocompatible or not in the human biological system. The biocompatibility of certain material usually carried out according to reported standards (ISO 10993) series or analogous, and the level and time interval of the adverse biological reaction will be measured. It does not determine biocompatibility, but it is a great step toward testing the material in the animal's physiological system. Finally, after that acknowledged the material do not induce any adverse reaction in the body of the recipient, then material became use in medical applications [32]

2. BIOCERAMICS

Bioceramics materials are the group of developed ceramics, refractory polycrystalline compounds using in repairing and rebuilding of the damaged or diseased tissues in the human's musculoskeletal system [33]. The use of materials in surgery implants before 1925, extensively included pure metals. In 1930, the metallic alloy has been used in surgical implants such as Vitallium. The new materials in 1969 were found by L.L. Hench, he was found some glass and ceramics in which they can make a bond with the bone. The founded ceramics by L.L. Hench have started examination into these soldier's bodies in which injured in the Vietnam war, but some of the implants were rejected by the body. For this reason, Hench tried to investigate a material that would have biocompatibility. As a result, he was found bioglass, after finding bioglass the interest in bioceramics increased rapidly [34, 35]. Ceramics have been widely used for therapeutic purposes for a lot of years, owing to extremely required features, such as chemical stability, biocompatibility, and non-toxicity. Bioceramics use in medicine is limited for some load-bearing applications due to their hardness and brittleness property. Besides this, they have high compressive strength and high wear resistance, due to these properties it was accepted in dental repairing and some definite orthopedic employment as a part of a synthetic joint. Ceramics medical application includes bone defect repair, alveolar bridge maintenance, augmentation, hip joint implant, ear implant, etc. Additionally, they have been used in the drug delivery system, owing to their biocompatibility and resorbable property. Ceramic use in healthcare applications caused to save the life millions of humans or improved their life quality[32, 36]. Bioceramics can be classified into three different class in term of tissue response at implantation interface, as listed at Table.2.1.

Table 2.1. Classification of bioceramics in term of their tissue attachment [33, 37].

	Class	Example	Form of attachment
1)	Inert	Alumina, zirconia	Connect tissue growth to surface defect by cementing or pushing to defect. (Morphological Fixation)
2)	Bioactive	Bioactive glass-ceramics, Bioactive glasses, HAp	Interfacially making the bond with the tissues. (Bioactive Fixation)
3)	Bioresorbable	Bioactive glasses, Tri-calcium phosphate, calcium sulfate	Slowly degrading and replacing by the tissue cells.

2.1. Types of Ceramics

Due to their structural function and properties, bioceramic can be classified into three types (inert bioceramics, bioactive bioceramics, biodegradable bioceramics) [33].

2.1.1. Inert Bioceramics

Bioinert ceramics are those ceramics, in which not react with the host tissue during implanted in the live system since they have chemical stability. There are two most important types, Alumina (Al_2O_3) and Zirconia (ZrO_2). They reveal interest mechanical properties, great bending, and compressive strength and better biocompatibility rather than Cobalt-Chrome alloy or stainless steel. The physical and mechanical properties of inert bioceramics are shown in Table 2.2. Due to desire properties alumina for the first time in the 1980s were used for artificial bone and joint implants [38]. With regarding their crystallographic stability, alumina ceramic completely has a hexagonal crystal structure that provides it most chemical stability as implanted in the human body. While zirconia includes three crystallographic phases; cubic, monoclinic, and tetragonal. The phase change occurs due to several circumstances such as mechanical stress, variation in temperature, and moisture. Sometimes self-damage of the ceramic occurs due to the phase change [39].

Table 2.2. Physical and mechanical properties of zirconia and alumina [19, 40].

Properties	Zirconia (ZrO_2)	Alumina (Al_2O_3)
Flexural strength, (GPa)	1,2	0.4 - 0.55
Young modulus, (MPa)	2×10^5	3.8×10^5
Hardness, (Mohs)	6.5	9.0
Fracture toughness, K_{1C} (Mpa.m$^{-1/2}$)	15	5 – 6
Grain size, (μm)	6.0	4.0
Surface roughness, R_a (nm)	8	20
Density, (g/cm^3)	5.60 - 6.12	3.90 -3.93

2.1.2. Bioactive Ceramics

Bioactive ceramics are those ceramics in which directly making the bond with the host tissue as implanted into the living system. Extremely, the bioactive materials are built on ceramics, glass or glass-ceramics encompass calcium (Ca) and silicon (Si) ions or calcium phosphates (CAP) such as HAp. For the first time, the ability to employ glass in the body for bone healing was studied by Larry Hench in fifty years ago. The direct bond of the host tissue with the implanted materials occurs by producing a bioactive carbonate-hydroxyl film, in which it is identical to the inorganic composition phase of bone, that tolerate the interfacial bond [41, 42]. The glass-ceramic A-w, exhibit better mechanical properties such as (bending strength, young modulus, and fracture toughness) over other glass and glass-ceramics that exist in medical application. This provides capability glass-ceramics to be used in some load-bearing compression field in bony orthopedics. The efforts to promote bioactive ceramic applications were concentrated mainly on two fields. First, prepare (organic-inorganic) mixtures to employ in tissue engineering and coatings on the surface of metallic materials for the applications that demanding noble mechanical properties. Second, prepare porous material with a perfect bioactive response that can be improved by incorporating biological molecules or inorganic therapeutic ions to be employed in hard tissue engineering [43]. The material bioactivity rate can be classified into two classes in terms of their index of bioactivity (*IB*). 1) Materials with an *IB* value of greater than 8 such as (glass-ceramic and bioactive glass), actively react with tissues and cause intrinsic healing and regeneration and also bonding to hard and soft tissue. 2) Materials with *IB* value greater than 0 but smaller than 8 these materials are considered to be only osteoconductive such as (HAp and TCP) [44].

2.1.3. Biodegradable Ceramics

Biodegradable ceramics are those ceramics in which chemically broking down by the body fluid during implantation in vivo. Furthermore, the biodegradable ceramics interface with bone is not steady compare to the bioinert ceramics. There are more instances of biodegradable ceramics such as tricalcium phosphate (TCP), hydroxyapatite (HAp), octacalcium phosphate (OCP), Calcium phosphate salts (Caps). The degradation degree of calcium phosphates is depended on the pH of the medium and solubility of the material. It is different for any structure in the following order (HAp << β-TCP< α-TCP). The degradation degree of calcium phosphates is increasing with, an increase of surface area, crystal grain size decrease, decrease in crystallinity, and grain size decrease. In contrast decrease with, magnesium substituted into β-TCP, fluorine incorporated to HAp, and β-TCP/HAp. The calcium phosphates have been used for about thirty

years in medical applications such as periodontal repair, alveolar ridge growth, and maxillofacial surgery. There are just two-member calcium phosphates that have stability at human body temperature, dicalcium phosphate DCP at pH smaller than 4.2, and hydroxyapatite HAp at pH equal and greater than 4.2. There are definite compounds in calcium orthophosphate that can be used in medical applications, due to their stoichiometry Ca/P ratio as seen in Table 2.3. These calcium phosphates, which have a Ca/P ratio of below 1 cannot be used in medical applications. Since these lead to increment in solubility due to their acidity. Moreover, the Ca/P ratio directly affects the calcium phosphate's mechanical behaviors and the solubility rate [33, 35, 45, 46].

Table 2.3. Chemical formulas, (Ca/P) molar ratio, and solubility at 37°C of some calcium orthophosphate compounds [47].

Calcium phosphates	Chemical composition	Ca/P molar ratio	Rate of Solubility at 37°C
Monocalcium phosphate monohydrate (MCPM)	$Ca(H_2PO_4)H_2O$	0.5	Extremely soluble
Monocalcium phosphate anhydrous (MCPA)	$Ca(H_2PO_4)_2$	0.5	Extremely soluble
Dicalcium phosphate anhydrous (DCPA)	$CaHPO_4$	1.0	$9.2 \times 10^{-7}\ M^2$
Dicalcium phosphate dihydrate (DCPD)	$CaHPO_4\ 2H_2O$	1.0	$1.87 \times 10^{-7}\ M^2$
Octa calcium phosphate (OCP)	$Ca_8H_2(PO_4)_6 5H_2O$	1.33	$2.5 \times 10^{-99}\ M^{16}$
Amorphous calcium phosphate (ACP)	$Ca_xH_y(PO_4)_z \cdot nH_2O$, $n = 3–4.5$; 15–20% H_2O	1.20-2.20	Variable
α–Tricalcium phosphate (α-TCP)	α- $Ca_3(PO_4)_2$	1.5	$2.8 \times 10^{-29}\ M^5$
β- Tricalcium phosphate (β-TCP)	β- $Ca_3(PO_4)_2$	1.5	$2.5 \times 10^{-30}\ M^5$
Hydroxyapatite (HAp)	$Ca_{10}(PO_4)_6(OH)_2$	1.67	$5.5 \times 10^{-118}\ M^{18}$
Fluorapatite (FAP)	$Ca_{10}(PO_4)_6F_2$	1.67	$5.0 \times 10^{-123}\ M^{18}$

Among all calcium orthophosphates, Hydroxyapatite and Tricalcium phosphate are the most compromises with the medical application. The solubility of Hydroxyapatite is identical to the biological apatites. But compare to HAp, the solubility of TCP is very quick. That means HAp in the human aqueous medium has the most chemical stability. It is about two-decade calcium phosphate ceramics are used to bone and dentistry medicine. Because the main mineral constituent in these tissues is calcium phosphate. As a result, calcium phosphate used in hard tissue prosthesis such as middle ear surgery, spine surgery, head reconstructive surgery, Miscellaneous, filling defects [45, 48, 49]. Generally, there is a different behavior of calcium phosphate compounds where implanted in the biological system. For instance, hydroxyapatite HAp may require a century to be disappearing within implantation defect, while calcium sulfate dihydrate CSD may disappear after only weeks. There are three significant features in the implantation biodegradable ceramics in the boney substitution. The first feature is associated with the solubility of this ceramic in the body. A second feature associated with the quickness where the used ceramic to remove from the body. The third feature associated with the affinity to turn into a different compound through dissolution precipitation reaction. In general, the calcium phosphate ceramics sintering temperature occurs at 1000-1500 °C then passes through compaction to make a needed form. One of the greatest use of calcium phosphate ceramics is using in the porous structure. Because porous structure makes the bone growth in the pores of the implanted calcium phosphate, as a result, this can lead to interfacing between implanted ceramic and the bone. Finally, it is providing high mechanical stability to the prosthesis. For bone formation, the porous structure is used as a scaffold [45, 50-52].

2.2. Hydroxyapatite (HAp)

Calcium orthophosphates-based material has a great interest in substitute or repairing damaged parts of human hard tissues. Because the major component in human bone and teeth is the calcium phosphate (CAP). Among all calcium phosphates, hydroxyapatite HAp with chemical composition $Ca_{10}(PO_4)_6(OH)_2$ is the most preferred implant material used throughout therapeutic applications [19, 33, 53]. Hydroxyapatite with the stoichiometry of Ca/P=1.67 is the most important calcium phosphate in the human body since it is the most identical to the human hard tissue in composition and stoichiometry. Moreover, the structure of hydroxyapatite is also resembling the structure of natural bone [54]. It exhibits excellent biological response (high biocompatibility, osteoconductivity, osteointegration, bioactivity, non-toxicity) in the biological environment. Therefore, these desirable properties made it used in more medical implantation (bone orthopedic, dentistry, plastic surgery, and neurosurgery). The constituents of the natural bone about (69 wt%) are consists of hydroxyapatite and in the enamel of teeth is about (97 wt%). The component of hydroxyapatite is included calcium (Ca^{+2}), phosphate (PO_4)$^{-3}$ and hydroxyl (OH^-) which are closely packed and arranged in a hexagonal (HCP) system with space group $P6_3/m$, and the lattice parameters $a = b = 9.418$ nm, $c = 0.6884$ nm, and volume of unit cell $V = 0.5288$ nm^3 with angels $\alpha=\beta = 90°$ and $\gamma = 120°$, and its crystal structure has shown in Figure 2.1 [55, 56].
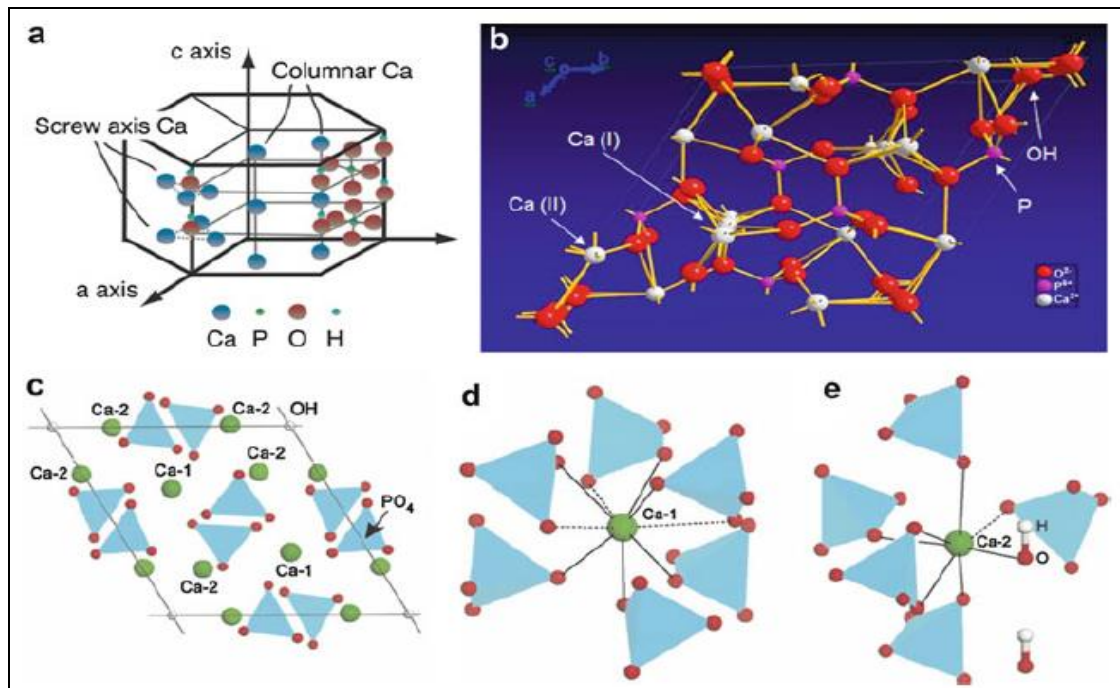
Figure 2.1. Crystal structure and ionic arrangement of the HAp.

Among all calcium phosphate ceramics HAp exhibits more stability under the thermodynamical condition like temperature, pH, and constitution of the human physiological environment it shows most stability rather than other calcium phosphate compounds. Due to its bioactivity property, it can inspire the bone to grow and repair. The restorative process in using HAp is faster compared to other materials used in this process. HAp at less than 1200 °C can remain in its structure, but above this temperature, it is decomposing into another phase called tricalcium phosphate (TCP). Also, the solubility hydroxyapatite HAp is more stable compared to calcium phosphate TCP, owing to their Ca/P ratio, 1.67 for HAp, and TCP is 1.33 [35, 57, 58]. Porosity is another important property of hydroxyapatite; HAp can exist in microporous or macroporous. Microporosity and macroporosity of the synthetic HAp dependent on the degree and duration of sintering temperature, high sintering temperature lead to a low degree of porosity. Due to this interesting surface properties, in bone implantation make the bone-bonding and growing within the pores, which give more stability for the implantation. Additionally, porous hydroxyapatite used in drug delivery, owing to its capability to degradation in aqueous medium [59, 60]. Hydroxyapatite exhibits poor mechanical properties; it makes the use of hydroxyapatite be limited to some load-bearing orthopedic applications. It is mechanical behaviors depend on some characteristics like sinterability, microstructure, grain size, and phase composition. The measured mechanical properties of HAp are given in Table 2.4 [33, 56].

Table 2.4. Typical mechanical properties of HAp [33, 56].

Properties	Value
Flexural strength	0.038–0.25 GPa
Compressive strength	0.12–0.15 GPa
Tensile strength	0.038-0.3 GPa
Young modulus	35-120 GPa
Vicker hardness	3-7 GPa
Weibull's modulus	5-18

Hydroxyapatite has anti-corrosion property, therefore in a macroporous and microporous form in some medical applications used as a coating to prevent the corrosion of metallic implant in the physiological system and providing more stability of the implanted prosthesis [61]. Hydroxyapatite related to the apatites, which have the capability of substituting foreign ions to its structure. Therefore it is substituting or co-substituting with both cationic and anionic foreign elements to controlling its biocompatibility, microstructure, physicochemical and mechanical properties [12]. One of the most trace elements that can be doped into HAp structure is strontium (Sr).

Strontium (Sr), is a trace micro-element that exist in bone and teeth, 99% of it is amount accumulated at a bone. Even its small amount of existence has a great role in the human body. Sr is one of the greatest efficient elements for bone cancer, osteoporosis, and bone pain release. Further, Sr influences reducing the osteoclast differentiation and rise activity of the osteoblast. Additionally, Sr deficiency cause to increase in bone resorption and deliberate bone formation process. Additionally, strontium has antibacterial property, therefore used with fluorine in the treatment of tooth decay. The bending strength and young modulus of Sr are higher than the HAp. As a result, incorporation of the Sr into HAp has been reported by many researchers that can improve the HAp microstructure, bioactivity, and mechanical properties [14, 62-64]. Erbium (Er), is one of the rare earth elements. The highest quantity of erbium in the human body exists at the bone and the lower quantity at the liver. It has great biocompatibility and can enhance biological properties for hydroxyapatite. It has been revealed the Er can affect the bone healing process. Er is non-toxic, bioactive, and biocompatible, therefore it is interested in medical applications [17, 65].

3. MATERIAL AND METHOD

In this section, the experimental procedure is given step by step. Then, the characterization process is clarified together with introducing the as-used devices and experimental conditions.

3.1. Experimental Procedure

The wet chemical method used to synthesize HAp samples co-doped with Sr and Er were synthesized by using a wet chemical method. While Sr-content was fixed with a constant amount of 0.35 at % for each sample and Er was added in five various amounts as (0, 0.35, 0.70, 1.05, and 1.40 at %). The used solvent for prepared samples was distilled water. A 100 mL of (0.5-x-y) M calcium nitrate tetrahydrate (Ca $(NO_3)_2 \cdot 4H_2O$, Carlo-Erba), x M strontium nitrate (Sr $(NO_3)_2$, Sigma Aldrich) and y M erbium nitrate pentahydrate ($Er(NO_3)_3 \cdot 5H_2O$, Sigma Aldrich) were dissolved in a beaker in the distilled water. Here, he Sr amount for each sample represented by x and equals the value of 0.35 at *%*. Er amounts are represented by y and equal to the values of 0, 0.35, 0.70, 1.05, and 1.40 at.%. While, in another beaker, a 100 mL of 0.3 M di-ammonium hydrogen phosphate (($NH_4)_2HPO_4$, Merck, Germany) solution was prepared, then drop by drop spilled into Ca $(NO_3)_2 \cdot 4H_2O$, $Sr(NO_3)_2$ and $Er(NO_3)_3 \cdot 5H_2O$ solution. Then, the milky white solution was gained. The pH value for all aqueous solutions was adjusted to 9.5 by adding an aqueous solution of ammonium hydroxide (NH_4OH, Sigma Aldrich) drop wisely. Every mixture was stirred by a magnetic stirrer for 90 min at room temperature and a gel formation was observed. Then, in an oven at 135 °C for 19 h this gel was dried. All dried samples in an electric furnace at 900 °C for 2 h were calcined and Sr/Er co-doped HAp samples in the powder form were obtained.

3.2. Characterizations

A Rigaku RadB-DMAX II device was used for XRD investigations. The patterns were exposed to Cu-Kα radiation using the wavelength (λ) of 0.15406 nm and measured at different angles between from 20° to 60° with a diffractometer operated at 40 kV and 40 mA. PerkinElmer Spectrum One spectrometer used to Fourier transform infrared (FTIR) measurements within the range from 400 to 4000 cm^{-1}, with using pellets of potassium bromide (KBr). For analyzing the morphology and the elemental compositions of the samples, a scanning electron microscope (SEM, FEI Quanta 450 FEG) equipped with an energy dispersive X-ray (EDX, Amatek Octane Plus) operated at 20 kV. Shimadzu DTA 50 was used to performing Differential thermal analysis. Furthermore, the samples thermal properties in the range from 25 to 1000 °C at a heating rate of 10 °C min^{-1} were studied. The density of states and band structure of the samples were studied by using Quantum Espresso software and density functional theory.

4. RESULTS AND DISCUSSIONS

In this part of the thesis, the results obtained from the characterization of all the samples are discussed in more detail. Moreover, the reason for each obtained result is compared with the reported studies and available data in the literature.

4.1. X-Ray Diffraction (XRD) Analysis Results

The X-ray diffraction patterns of all synthesized samples are presented in Figure 4.1. From the X-ray diffraction patterns, the detected phase for all samples is HAp (JCPDS no: 09-0432), no secondary phase can observe. From the (XRD) graphs, the change in peaks intensities can be observed due to the addition of Er^{3+} in various amounts. That may attribute, to the addition the foreign ion whose in ionic radius differs from that of calcium. Additionally, that might due to the difference in electron density of the substituted atom with atoms at the surround, which can make some peaks more intense and other peaks less intense [66]. The inter planer distance (d) and (2θ) values for each peak as detected on the XRD patterns were measured as listed in Table 4.1. As can be seen in the table, the addition of Er in various amounts caused the increase and /or decrease in (2θ) and (d) values. These changes can be explained as follows, the element with the smaller ionic radius Er^{3+} (0.088 nm) substituted to the larger ionic radius element Ca^{2+} (0.099 nm) can cause a change in lattice parameters and induce the lattice strain, i.e compressive stress decrease in 2θ, tensile stress increase in 2θ. Additionally, as well reported, change in lattice parameters due to enhance surface forces that can cause a change in d values [67-69].
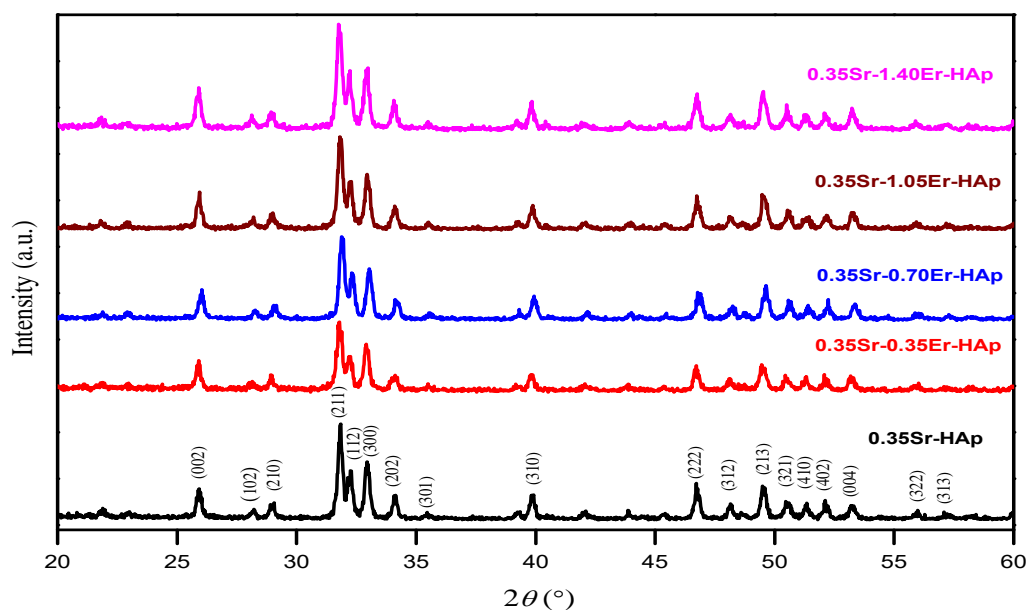
Figure 4.1. XRD patterns for free of Er and doped Er to Sr-based HAps.

Table 4.1. The measured value of the interplanar distance d and 2θ for all peaks.

Sample	Miller indices				
	h	k	l	2θ (°)	d (nm)
0.35 Sr-HAp	0	0	2	25.918	0.34345
	1	0	2	28.218	0.31650
	2	1	0	29.059	0.30808
	2	1	1	31.839	0.28110
	1	1	2	32.262	0.27742
	3	0	0	32.939	0.27170
	2	0	2	34.139	0.26262
	3	1	0	39.918	0.22606
	2	2	2	47.716	0.19411
	2	1	3	49.500	0.18377
	0	0	4	53.199	0.17172
0.35 Sr-0.35 Er-HAp	0	0	2	25.899	0.34374
	1	0	2	28.139	0.31672
	2	1	0	28.920	0.30824
	2	1	1	31.799	0.28126
	1	1	2	32.259	0.27760
	3	0	0	32.919	0.27184
	2	0	2	34.119	0.26279
	3	1	0	39.799	0.22618
	2	2	2	46.719	0.19422
	2	1	3	49.459	0.18389
	0	0	4	53.179	0.17185
0.35 Sr-0.70 Er-HAp	0	0	2	26.039	0.34194
	1	0	2	28.279	0.31514
	2	1	0	29.039	0.30716
	2	1	1	31.987	0.28019
	1	1	2	32.299	0.27632
	3	0	0	33.039	0.27089
	2	0	2	34.119	0.26161
	3	1	0	39.939	0.22539
	2	2	2	46.779	0.19344
	2	1	3	49.639	0.18304
	0	0	4	53.360	0.17095

Table 4.1. The measured value of the interplanar distance *d* and 2*θ* for all peaks (Continued)**.**

Sample	Miller indices			2*θ* (°)	*d* (nm)
	h	*k*	*l*		
0.35 Sr-1.05 Er-HAp	0	0	2	25.939	0.34320
	1	0	2	28.199	0.31630
	2	1	0	28.999	0.30808
	2	1	1	31.819	0.28106
	1	1	2	32.265	0.27729
	3	0	0	32.940	0.27170
	2	0	2	34.100	0.26251
	3	1	0	39.789	0.22606
	2	2	2	46.739	0.19406
	2	1	3	49.486	0.18368
	0	0	4	53.219	0.17162
0.35 Sr-1.40 Er-HAp	0	0	2	25.899	0.34372
	1	0	2	28.119	0.31664
	2	1	0	28.940	0.30772
	2	1	1	31.761	0.28086
	1	1	2	32.239	0.27744
	3	0	0	32.980	0.27138
	2	0	2	34.059	0.26261
	3	1	0	39.839	0.22580
	2	2	2	46.759	0.19400
	2	1	3	49.519	0.18378
	0	0	4	53.240	0.17185

To calculate the crystallite size values for all samples, the Scherrer (D_S) and Williamson-Hall (D_{WH}) equations were used [70, 71].

$$D_S = \frac{0.9\lambda}{\beta\,Cos\,\theta} \tag{4.1}$$

$$\beta\,Cos\,\theta = \frac{0.9\lambda}{D_{WH}} + 4\varepsilon\,\sin\theta \tag{4.2}$$

Here β represented the full width at half maximum (FWHM), λ is the wavelength of incident X-ray source ($\lambda = 0.15406$ nm), ε is the lattice strain, and θ is the angle of diffraction.

The values of D_{WH} obtained from the y-intercept of the Figure 4.2. as plotted as $\beta cos\theta$ vs $4sin\theta$ for all prepared samples as shown in, and the lattice strain ε value gives from the slope of the figure.

The equation 4.2. can be rearranged with using this relation $\varepsilon = \sigma / Y$, the equation 4.3 can be obtained [72].

$$\beta\,cos\,\theta = \frac{0.9\lambda}{D_{WH}} + \frac{4\sigma\,\sin\theta}{Y} \tag{4.3}$$

Where σ is representing the stress and Y_{hkl} is Young's modulus, the slope of the Figure 4.3. as plotted as $\beta\,cos\,\theta$ against $4sin\,\theta\,Y^{-1}$ for all Miller indices were detected on XRD patterns gives the σ values of all samples.

The Young's modulus (Y) can be calculated by using the following equation 4.4 [73].

$$Y = \frac{\left(h^2 + \frac{(h+2k)^2}{3} + \left(\frac{al}{c}\right)^2\right)^2}{s_{11}\left(h^2 + \frac{(h+2k)^2}{3}\right)^2 + s_{33}\left(\frac{al}{c}\right)^4 + (2s_{13} + s_{44})\left(h^2 + \frac{(h+2k)^2}{3}\right)\left(\frac{al}{c}\right)^2} \tag{4.4}$$

Here both a and c are the lattice parameters. The elastic compliance values are represented by s_{11}, s_{33}, $s_{13,}$ and s_{44}, their standard values are reported as 7.49×10^{-12}, -4.0×10^{-12}, $10.9\times10^{-12,}$ and 15.1×10^{-12} m^2 N^{-1} individually. The anisotropic energy density (u) can be estimated, by using relation $(2u/Y)^{1/2}$ instead of ε in modified equation 4.2.

$$\beta\,cos\theta = \frac{0.9\lambda}{D_{WH}} + 4\,sin\,\theta\left(\frac{2u}{Y}\right)^{\frac{1}{2}} \tag{4.5}$$

For all of the synthesized samples, u value can be obtained by using the slope of the Figure 4.4. as plotted between $\beta\,cos\theta$ vs $2^{5/2}\,sin\,\theta\,Y^{-1/2}$.
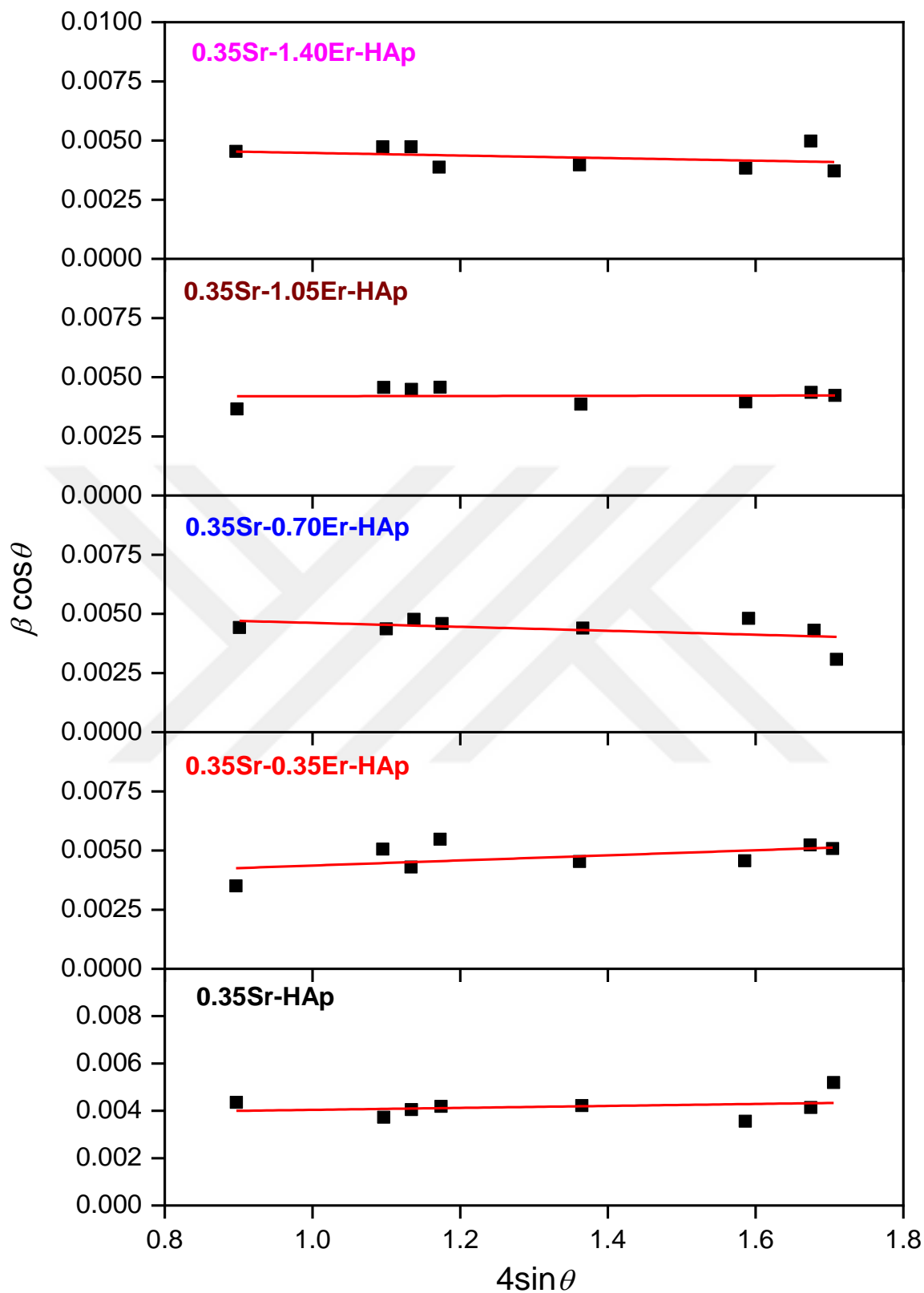
Figure 4.2. The graph of $\beta \cos \theta$ against $4 \sin \theta$ for all prepared samples.
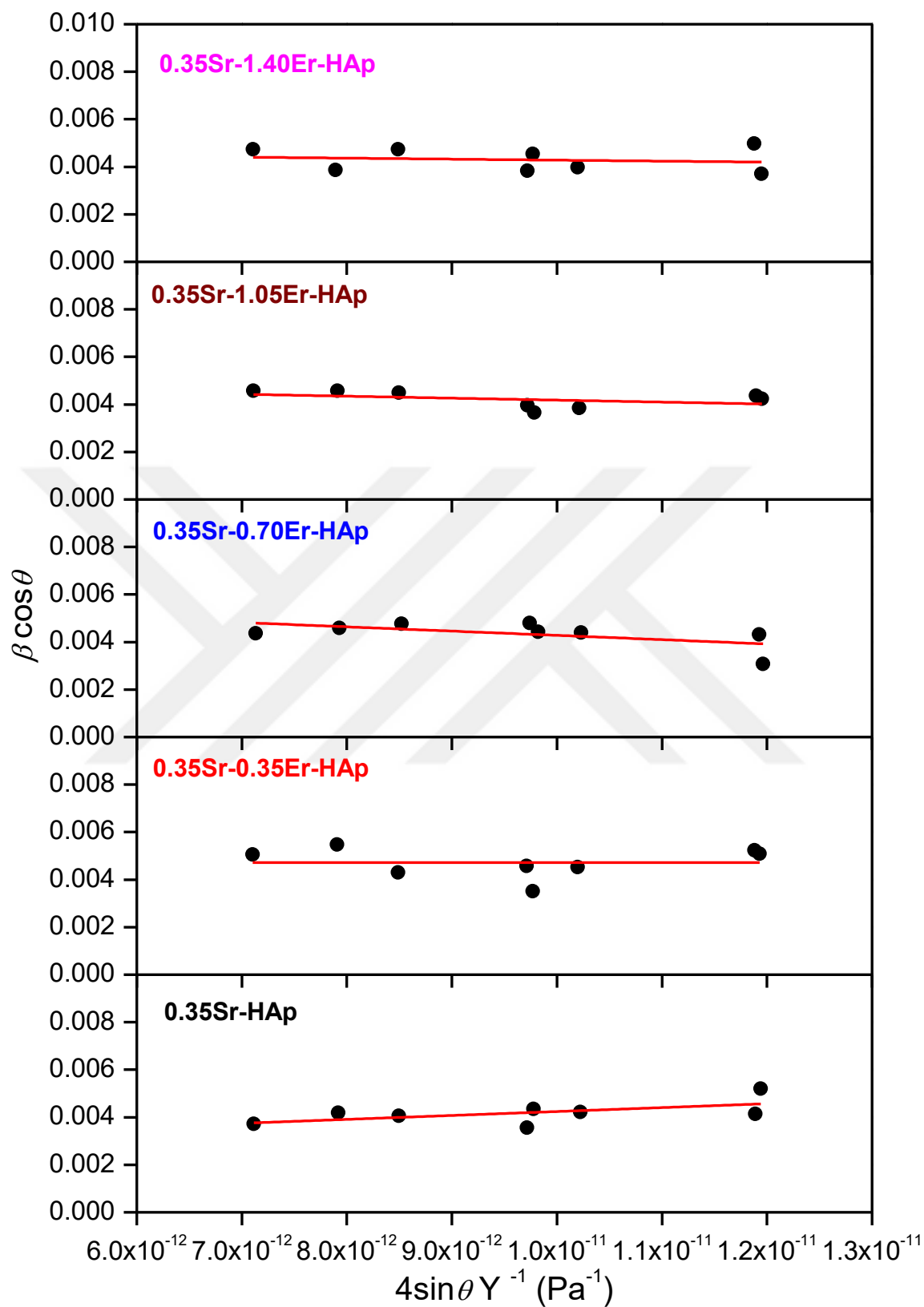
Figure 4.3. The plotted graph of β cos θ against 4sin θ Y^{-1} for as-synthesized samples.
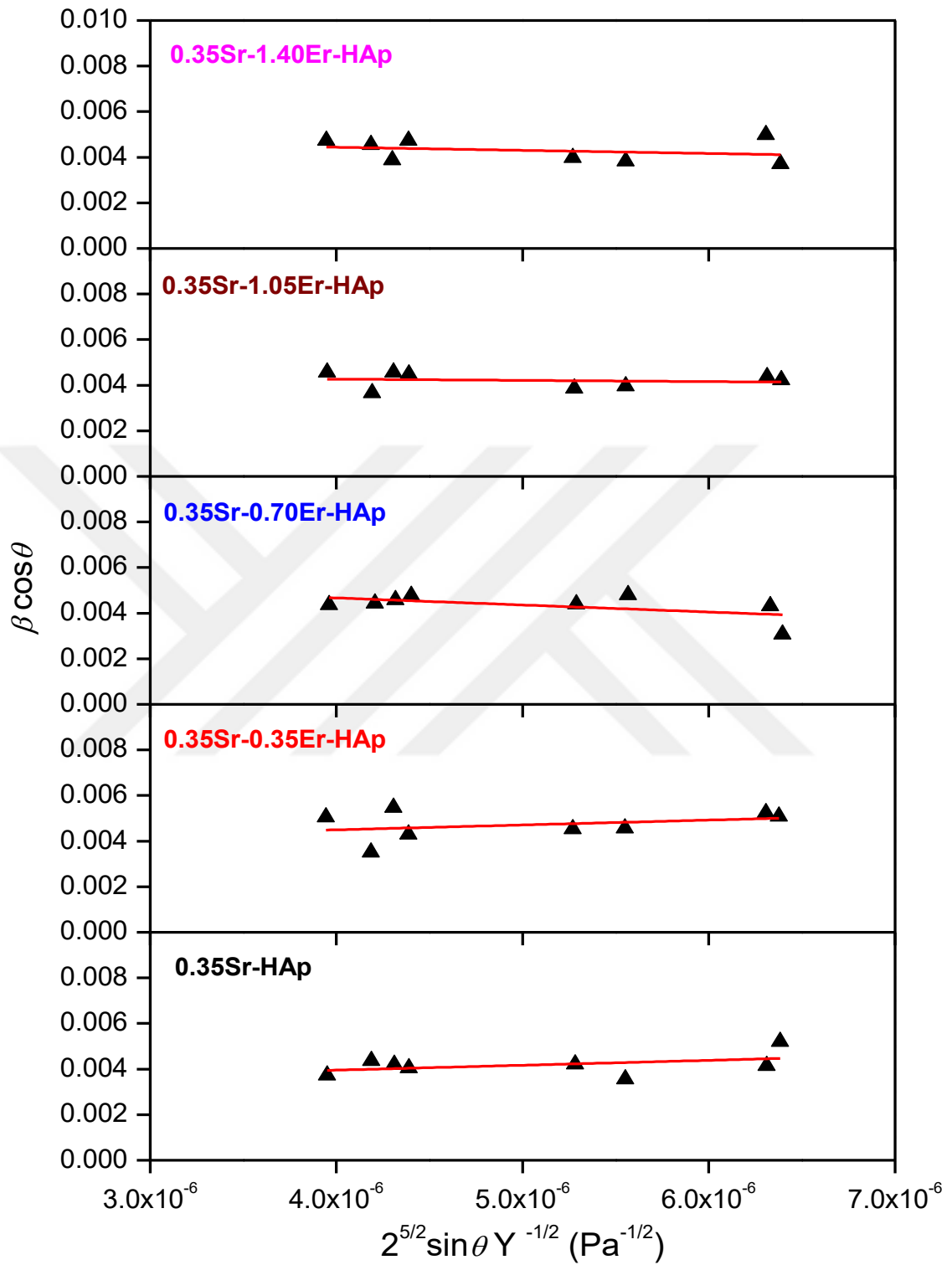
Figure 4.4. The plotted graph of $\beta \cos\theta$ vs. $2^{5/2} \sin\theta \, Y^{-1/2}$ for all samples.

For all synthesized samples, the values of the lattice parameters (*a* and *c*) and the volume of the unit cell (*V*) for all synthesized samples were calculated via applying the following relations [70].

$$\frac{1}{d^2} = \frac{4}{3}\left(\frac{h^2 + hk + k^2}{a^2}\right) + \frac{l^2}{c^2} \tag{4.6}$$

$$V = \frac{\sqrt{3}}{2}a^2c \tag{4.7}$$

Where d is interplanar distance.

The crystallinity percentage (X_C %) for each sample was estimated by using the following relation [70].

$$X_C\% = \frac{\sum A_c}{\sum A_c + \sum A_A} \tag{4.8}$$

Where $\sum A_C$ represents the entire area under crystal peaks, and $\sum A_A$ represents the entire area below amorphous peaks. Also in keeping with Landi et al.[74], the crystallinity percentage (X_{CL} %) was calculated by using the following relation.

$$X_{CL}\% = \left(1 - \frac{V_{112/300}}{I_{300}}\right) \times 100 \tag{4.9}$$

Where $V_{112/300}$ is the intensity of the pit between (112) and (300) reflections and I_{300} is the intensity belonging to (300) reflection.

Table 4.2. The parameters calculated from the XRD analysis for all samples.

Sample	0.35Sr-HAp	0.35Sr-0.35Er-HAp	0.35Sr-0.70Er-HAp	0.35Sr-1.05Er-HAp	0.35Sr-1.40Er-HAp
D_S (nm)	34.23	32.23	29.07	30.91	29.27
D_{WH} (nm)	38.20	42.14	25.44	33.41	27.62
a (nm)	0.9412	0.9417	0.9384	0.9412	0.9401
c (nm)	0.6869	0.6874	0.6838	0.6864	0.6874
V (nm^3)	0.5270	0.5279	0.5215	0.5266	0.5261
X_C%	91.4	90.9	90.5	90.4	89.1
X_{CL}%	93.65	90.39	90.18	89.26	89.05
ε	0.42×10^{-3}	1.08×10^{-3}	-0.84×10^{-3}	0.04×10^{-3}	-0.54×10^{-3}
σ (MPa)	164.47	176.70	-180.25	-82.04	-41.44
u (kJ m^{-3})	46.37	45.60	98.91	2.96	18.53

The results were obtained from the analysis of XRD graphs are shown in Table 4.2. The following contribution can be reached. With the increase in Er content, the small reduction in crystallite sizes was observed for both Scherrer (D_S) and Williamson-Hall (D_{WH}) [70, 75]. Meanwhile, the substituting small ionic radius Er^{3+} (0.088 nm) to larger ionic radius Ca^{2+} (0.099 nm), some decreases in crystallite size value can be observed. On the contrary, an increase in the crystallite size is also observed, and this may be related to the alteration in the crystal lattice of HAp structure as a result of producing the lattice strain [76]. The gradual decrease in the crystallinity percentage (X_C %) and (X_{CL} %) has been observed with an increase in Er content. that means the erbium entered the apatitic structure and produced the defect. These results are in line with the results obtained by Alshemary et.al.[68]. The gradual increase or decrease did not detect for the lattice parameters (*a* and *c*), and the volume of unit cell (*V*) values. That can be clarified as follows, as the probability of substitution, the substitution ranges of Er^{3+} changed from one sample to another one, or may associate to the influence of carbonate substitution as substituted in PO_4^{3-} or OH^- into HAp lattice. The results are in good harmony with the results reported by Gamal et al.[77]. Besides, the obtained lattice strain values for all samples are influenced by Er^{3+} contents as can be seen in Table 4.2. The achieved negative value of lattice strain means that the unit cell under compressive stress and the positive value belong to the tensile stress. The results are in good agreement with the results obtained by Moghadam et al. [78]. Moreover, the stress (σ) and anisotropic energy density (*u*) values were also affected by Er doping for all samples as exposed in Table 4.2. The stress value decreased with an increase in Er content without the sample with 0.35 at% Er which increased, because of its proportionality with the strain. An increase in anisotropic energy density values of all samples were observed, just for the sample with 1.05 at% Er was decreased in comparision with their values of pure (HAp $\sigma = 52$ MPa and *u* = 12 kJm^{-3}) as stated by Venkatewarlu et al. [79].

4.2. Fourier Transform Infrared (FTIR) Spectroscopy Investigation

The FTIR spectra for all Sr-based HAps with various amounts of Er are presented in Figure 4.5. For all samples the bands belonged to the phosphate (PO_4^{3-}) group were found at 1087, 1024, 599, and 564 cm^{-1} wherein related to the symmetrical bending and stretching mode υ_3 and υ_4 of the PO_4^{3-} group. Also, the two bands located at 962 and 473 cm^{-1} ascribed the symmetric-stretching υ_1 and υ_2 of the phosphate (PO_4^{3-}) group individually. Additionally, the bands that correspond to the vibration modes of the hydroxyl (OH^-) group were obtained at 3572 and 630 cm^{-1}. A small band was detected at 1455 cm^{-1} matched the B-type substitution of carbonate (CO_3^{2-}) group, as well as, the band was found at 1408 cm^{-1} matched the A-type substitution carbonate (CO_3^{2-}) group [68, 80]. Additionally, the phosphate group band intensity was decreased for all

samples, which may be attributed to vibrational modes weakening (P-O and O-P-O) that results in a change in bonding forces, which that between amongst ions occur [81].
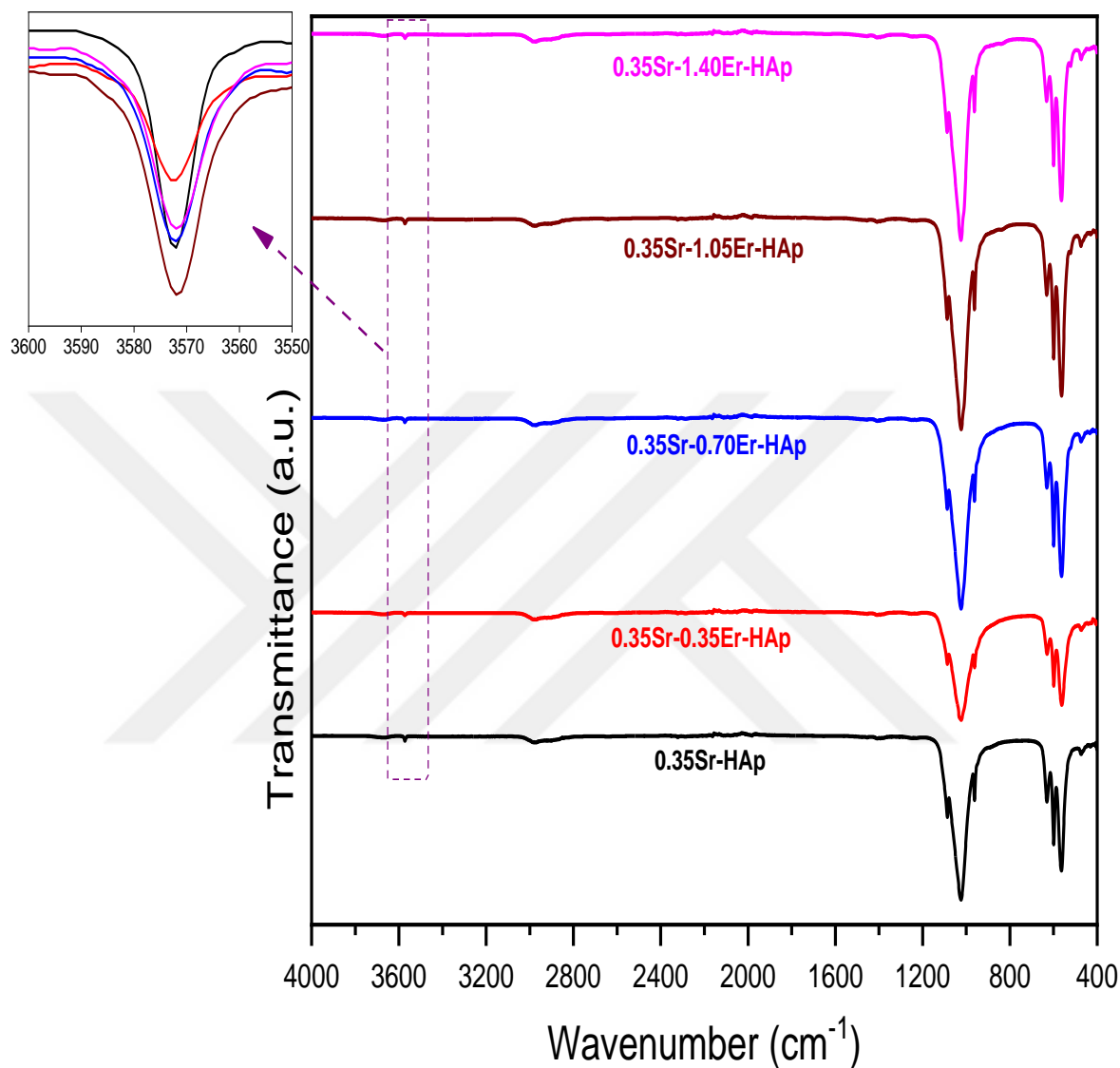
Figure 4.5. FTIR spectra of all synthesized samples.

4.3. Thermal Analysis

The differential thermal analysis (DTA) results for all prepared samples are shown in Figure 4.6. From the figure as can be seen clearly, it appears to be there is no significant change in the thermal properties of all samples in the temperature range 25 $^{\circ}$C – 1000 $^{\circ}$C. This indicates that the thermal stability did not affect by the co-dopants.
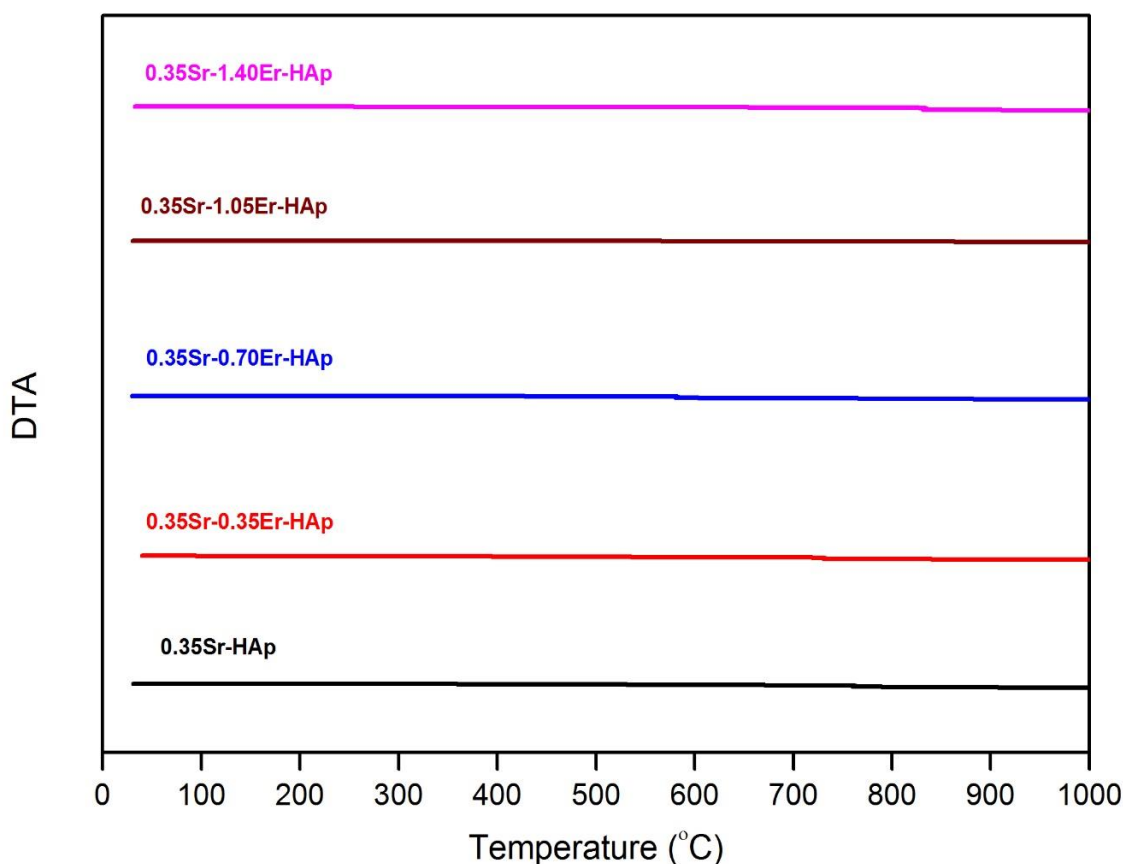
Figure 4.6. DTA analyze graph for all synthesized samples.

4.4. Morphological Analysis

The SEM micrographs and EDX analysis results for all synthesized samples are shown in Figure 4.7. As can be observed, all samples appeared to have a porous and agglomerated structure made out of sphere-like particles, the morphology of all samples almost identical. That indicates the amount of the dopant of almost did not cause the change in the morphology. The EDX spectra taken for as-synthesized samples exhibited that there is no impurity associated with any other element. The EDX recorded data confirmed that with an increase in Er content calcium deficiency has occurred. The (Ca + Sr +Er)/P molar ratio were found to be**,** 1.67 for 0.35Sr-HAp, 1.64 for 0.35Sr-0.35Er-HAp, 1.65 for 0.35Sr-0.70Er-HAp, 1.61 for 0.35Sr-1.05Er-HAp, and 1.63 for 0.35Sr-1.40Er-HAp. The values and theoretical value of stoichiometric HAp (1.67) are quite close.

0.35Sr-HAp

Element	Atomic %
Ca	21.81
Sr	0.08
P	13.05
O	65.06

0.35Sr-0.35Er-HAp

Element	Atomic %
Ca	21.53
Sr	0.08
Er	0.07
P	13.15
O	65.17

0.35Sr-0.70Er-HAp

Element	Atomic %
Ca	20.96
Sr	0.09
Er	0.15
P	12.82
O	65.98

0.35Sr-1.05Er-HAp

Element	Atomic %
Ca	20.17
Sr	0.07
Er	0.23
P	12.65
O	66.88

0.35Sr-01.40Er-HAp

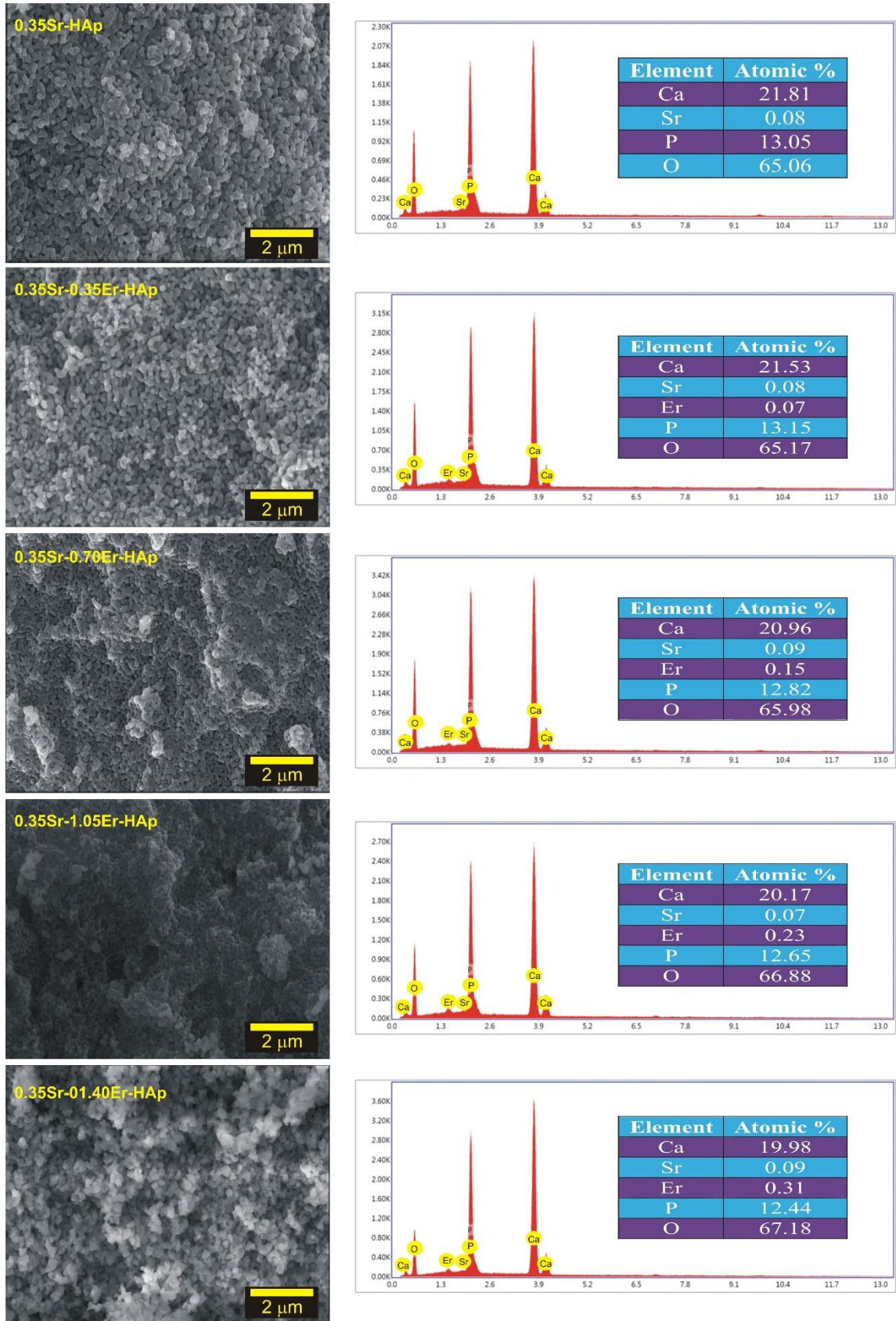| Element	Atomic %
Ca	19.98
Sr	0.09
Er	0.31
P	12.44
O	67.18

Figure 4.7. SEM images and EDX analysis result for all synthesized samples.

4.5. The *In Vitro* Cytotoxicity Investigation

The *in vitro* cytotoxicity values of all samples were tested on the mouse (*Mus musculus*) fibroblast cells (L-929), using the indirect method with MTT (thiazolyl blue tetrazolium blue) test using spectrophotometry. Following the "Biological Evaluation of Medical Devices" standards (ISO-10993-5) and test, the protocol was prepared. In the first step, the samples with 70% ethanol washed one time and with sterile PBS (pH 7.4) three times. Then, in an incubator with 37 °C and 5% of CO_2 the samples were incubated in the *DMEM* (Dulbecco's Modified Eagle's Medium) environment for 72 hours. The fibroblast Cell lines were grown in the incubated medium. They were separated from the flasks with the 0.25% trypsin-EDTA dissolvent. Afterward, the removed cells were centrifuged at 2000 rpm for 5 minutes and seeded as 10^4 cells / well into 96-well plates and incubated under the same conditions for 24 hours. In the last incubation time, the further 24-hour incubation time for the samples was used to replace the DMEM medium with the medium in which the samples were held for 72-hours. Then, the medium removed through the cells by addition 90 µL of fresh *DMEM* medium into the seeded plates. Furthermore, the cells incubated in dark for a further 4 hours under the same circumstances after the addition of 10 µL from 5 mg/mL MTT solution prepared with sterile phosphate-buffered saline into them. Consequently, using the ELISA microplate reader the absorbance values of the purple color at 550 nm was measured. For the control groups incubated under the same conditions, the medium kept in the incubator for 72 hours was inserted into wells and the cells in the wells were assumed to be 100% live. In consequence, the cell viability of the samples on L-929 cells was calculated as compared to the control groups as represented in Figure 4.8.
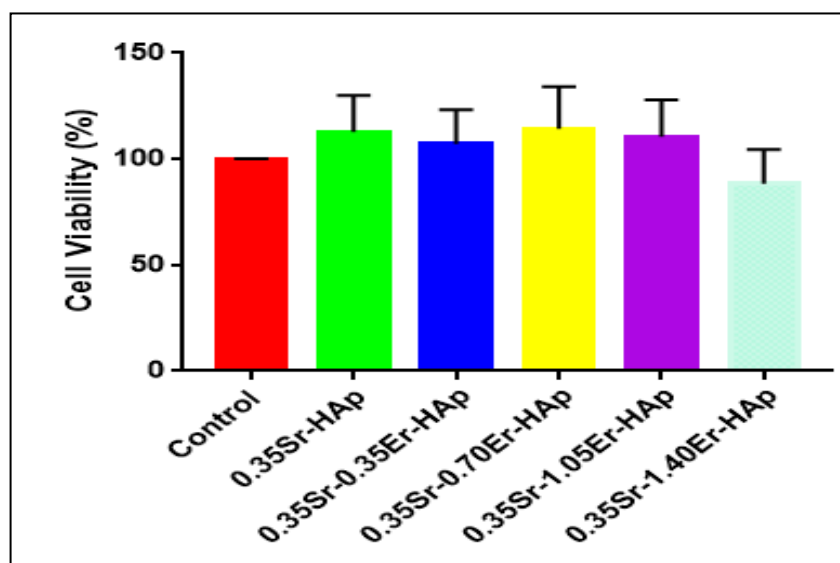
Figure 4.8. The cell viability of all synthesized samples.

27

According to the test results, the cell viability percentage of all samples in compare with the control group measured as; 112.86±17.25% for 0.35Sr-HAp, 107.10±16.22% for 0.35Sr-0.35Er-HAp, 114.27±19.93% for 0.35Sr-0.70Er-HAp, 110.48±17.42% for 0.35Sr-1.05Er-HAp, and 88.27±16.13% for 0.35Sr-1.40Er-HAp respectively. As can be observed all samples showed the cell viability higher than 85%, none of the samples exhibit cytotoxic effects over L-929 mouse fibroblast cells. This means that all of the synthesized samples are biocompatible materials and may adequate for medical purposes.

4.6. Investigation of Density of States and Band Structures

The principle of the density of the state is demonstrating that the electrons are allowed to be occupied at a different number of states at a particular energy level.

Here it is possible to achieve the electron density at each energy state by multiplying states number with the probability that an electron occupied a state. The density of states *DOS* as a function of energy has been estimated as,

$$DOS\ (E) = \sum g(E - \varepsilon_i) \qquad (4.10)$$

Where *g* displays a Gaussian with fixed full wave half maximum (FWHM), the energy of the ith molecular orbital represented as ε_i, and E represents the total energy.

The associated band structure and density of states spectrum for all free of erbium and doped erbium into HAp samples are shown in Figures 4.9-4.13. The quantum expresso software has been used to achieve simulation of all atomic calculations [82]. The density functional theory (DFT) has been used to achieve the bandgap energy among (HOMO-LUMO) which describes Higher Occupied Molecular Orbital and Lower Unoccupied Molecular orbital. The erbium free and erbium doped HAps obtained a bandgap between valence band which lies at the lower side and conduction band which lies at the upper side located at (*L-H*) point. For all samples as can be observed from the figures, the valence band surface and the conduction band surface have a nearly regular shape. Also as detected from the Figures the highest occupied point of the valence band and the lowest unoccupied point in the conduction band are located in the same wave vectors (*L-H*) position. This indicates that these materials described by a direct bandgap. While, as reported undoped HAp has an indirect-gap because the lower point of conduction band lies at k $= \Gamma$ and the maximum energy of valence band positioned at different wave vector as $\Gamma - M$ or

$\Gamma - K$ as reported by Avakyan.et al. [83]. The bandgap values for all samples are obtained as 5.1915 eV for 0.35Sr-HAp, 4.8835 eV for 0.35Sr-0.35Er-HAp, 3.9961 eV for 0.35Sr-0.70Er-HAp, 3.9197 eV for 0.35Sr-1.05Er-HAp and 3.9084 eV for 0.35Sr-1.40Er-HAp. These obtained

band gap values of all samples indicate that Er dopant content caused a decrease in band gap values as compared to the theoretical band gap energy value of pure HAp (5.23 eV) [84]. The decrease in bandgap could be demonstrated as follows: The energy level of Er^{3+} higher than the energy level of Ca^{2+}. Additionally, dissimilarity in electronegativity between Er^{3+} and Ca^{2+} also could be a cause the bandgap decreasing [85].
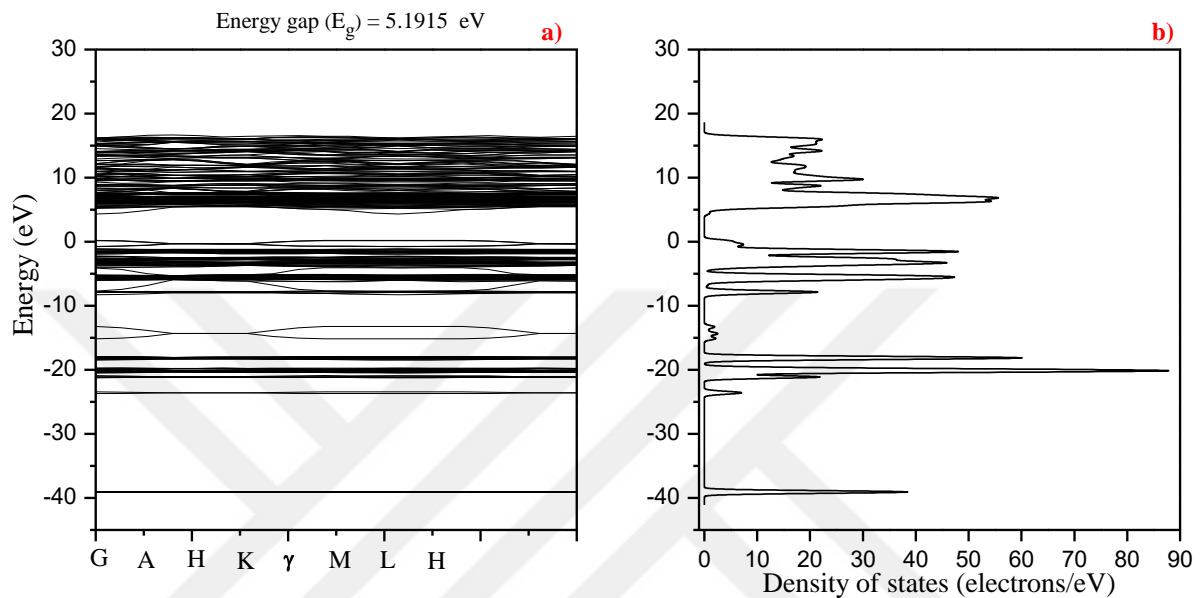
Figure 4.9. a) Band structure and b) density of states for 0.35Sr–HAp.
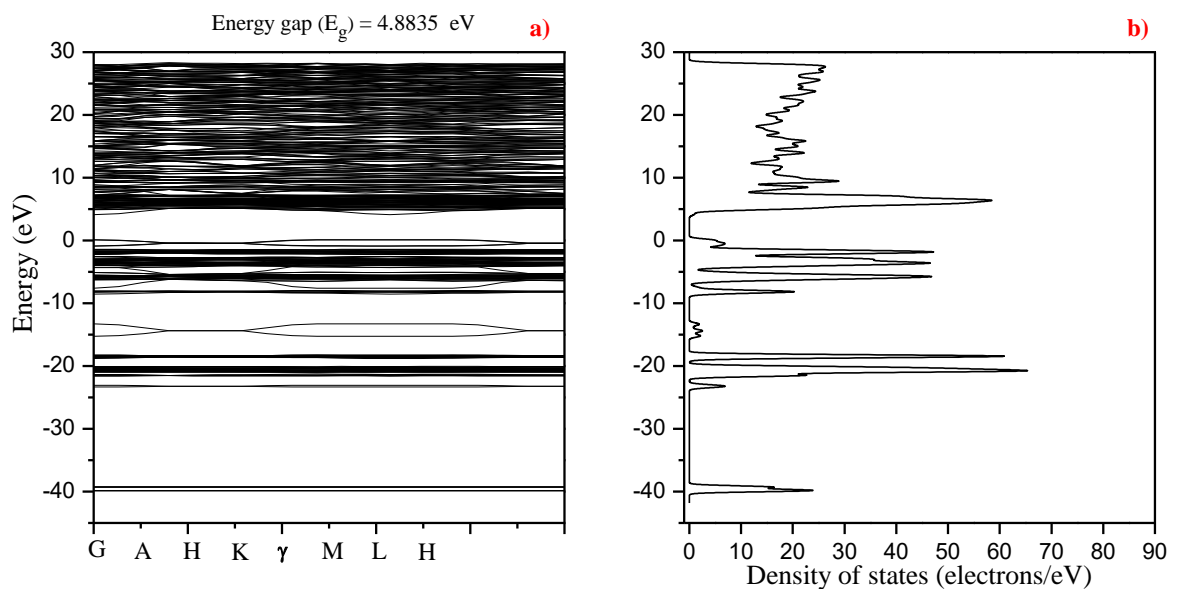
Figure 4.10. a) Band structure and b) density of states for 0.35Sr–0.35Er–HAp.
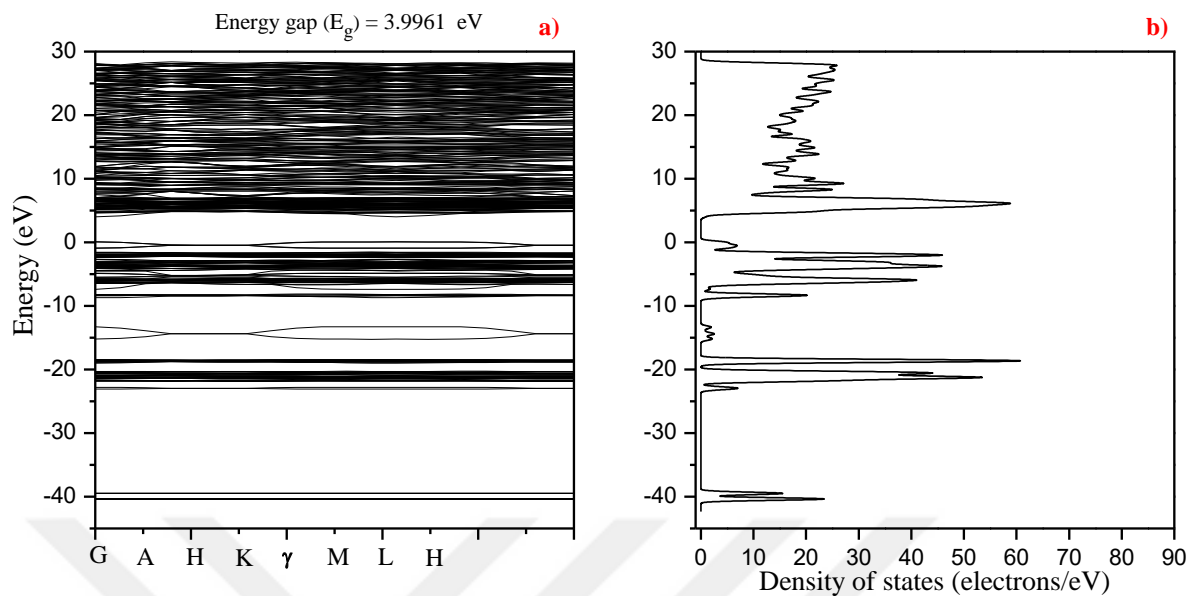
Figure 4.11 a) Band structure and b) density of states for 0.35Sr–0.70Er–HAp.

Figure 4.12. a) Band structure and b) density of states for 0.35Sr–1.05Er–HAp.

Figure 4.13. a) Band structure and b) density of states for 0.35Sr–1.40Er–HAp.
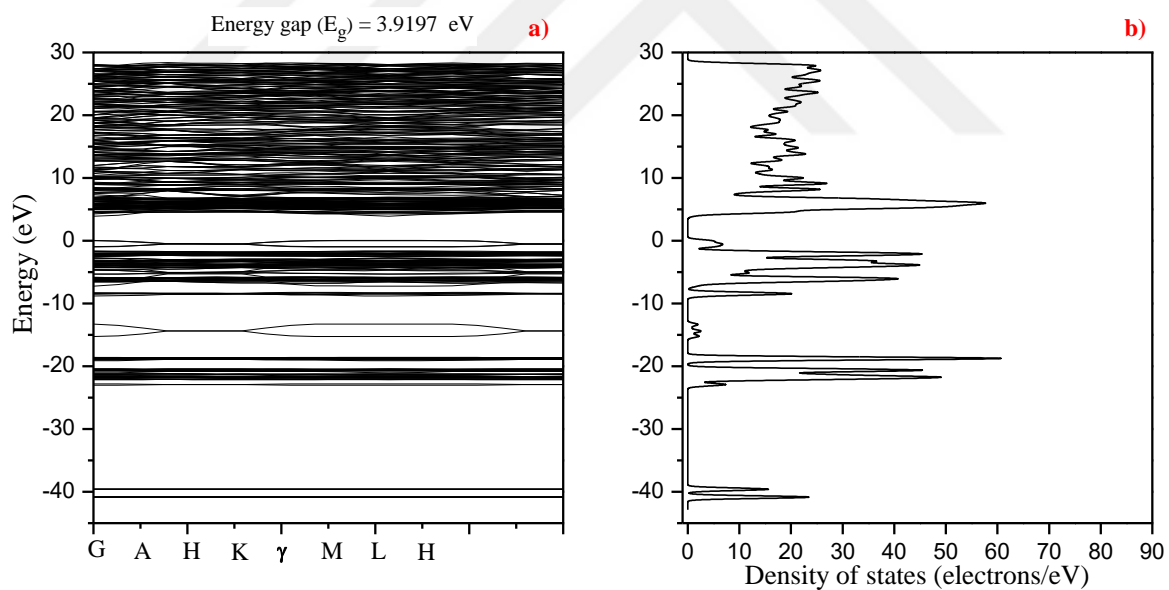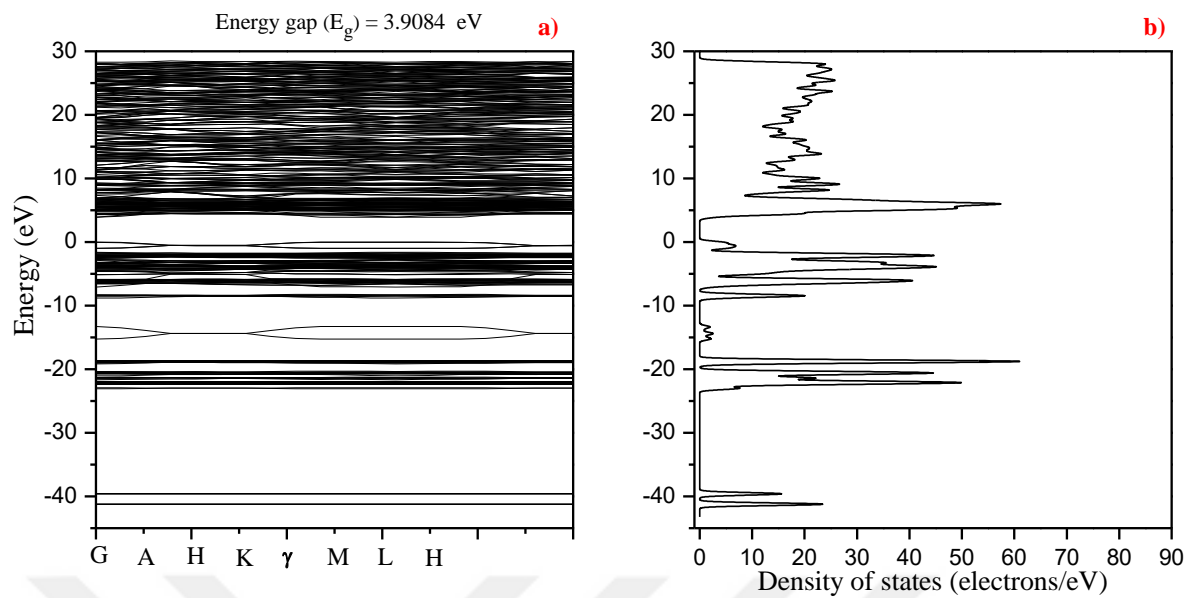
5. CONCLUSIONS

In this master's thesis, the Sr-based HAp samples containing various amounts of Er were synthesized via a wet chemical method. Their morphology, crystal structure, thermal properties and *in vitro* cytotoxicities were experimentally investigated, as well as, band structures and density of states theoretically and the following conclusions were reached;

- It is possible to synthesize HAp samples with low cost and high purity.
- With an increase in Er amount, gradual increase or decrease in lattice parameters did not observe.
- A gradual decrease in crystallinity percentage with an increase in Er concentration was observed.
- Er, doping to Sr-based HAp samples affected the lattice parameters (e.g. strain, stress, and anisotropic energy density).
- At the temperature range 25 to 1000 °C all prepared samples showed thermal stability in
- All prepared samples composed of sphere-like particles and has porous and agglomerated structures. No considerable changes can be observed in the morphology of the samples.
- The increase in Er concentration resulted in Ca-deficiency. The (Ca+Sr+Er)/P molar ratio for all samples was detected to be quiet close to the theoretical value (1.67)
- All synthesized samples did not exhibit cytotoxicity and all are biocompatible.
- The increase in Er concentration caused to narrowing band structures and bandgap energies decreased from 5.1915 eV to 3.9084 eV.

RECOMMENDATION

The following recommendations can be made for future studies:

- The amounts of the co-dopants can be changed.
- Another method (e.g., the sol-gel, combustion, spray pyrolysis, and so on) can be used for the synthesis of the samples.
- Transmission electron microscopy (TEM), dielectric measurements, inductively coupled plasma (ICP) technique, and Raman spectroscopy may be used for further characterization.
- The synthesis conditions can be changed.

REFERENCES

[1]   Steele, B.C. (2001). Material science and engineering: the enabling technology for the commercialisation of fuel cell systems, *Journal of Materials Science*, 36, pp.1053-1068.

[2]   LeGeros, R. (1993). An introduction to bioceramics, *Advanced Series in Ceramics,* 1(181), pp. 5-22.

[3]   Park, J.B., (2012). *Biomaterials science and engineering*, Springer Science & Business Media, pp. 1-10.

[4]   Huebsch, N. and Mooney, D.J. (2009). Inspiration and application in the evolution of biomaterials, *Nature*, 462, pp. 426-432

[5]   Ratner, B.D., Hoffman, A.S., Schoen, F.J., and Lemons, J.E., (2004). *Biomaterials science: an introduction to materials in medicine*, *MRC BUll*, 31, pp. 58-60.

[6]   Hench, L.L. (1998). Biomaterials: a forecast for the future, *Biomaterials*, 19, pp. 1419-1423.

[7]   Matassi, F., Nistri, L., Paez, D.C., and Innocenti, M. (2011). New biomaterials for bone regeneration, *Clinical cases in mineral and bone metabolism*, 8, pp. 21-24.

[8]   Lam, M.T. and Wu, J.C. (2012). Biomaterial applications in cardiovascular tissue repair and regeneration, *Expert review of cardiovascular therapy*, 10, pp. 1039-1049.

[9]   Parida, P., Behera, A., and Mishra, S. (2012). Classification of Biomaterials used in Medicine, International Journal of Advances in Applied Sciences (IJAAS), 1(3), pp. 31-35

[10]   Vallet-Regí, M. (2001). Ceramics for medical applications, *Journal of the Chemical Society, Dalton Transactions*, 2, 97-108.

[11]   Williams, D. (1976). Biomaterials and biocompatibility, *Medical progress through technology*, 4, pp. 31-42.

[12]   Kaygili, O., Dorozhkin, S.V., and Keser, S. (2014). Synthesis and characterization of Ce-substituted hydroxyapatite by sol–gel method, *Materials Science and Engineering: C*, 42, pp. 78-82.

[13]   Agrawal, K., Singh, G., Puri, D., and Prakash, S. (2011). Synthesis and characterization of hydroxyapatite powder by sol-gel method for biomedical application, *Journal of Minerals and Materials Characterization and Engineering*, 10, pp. 727-734.

[14]   Kaygili, O., Keser, S., Kom, M., Eroksuz, Y., Dorozhkin, S.V., Ates, T., Ozercan, I.H., Tatar, C., and Yakuphanoglu, F. (2015). Strontium substituted hydroxyapatites: synthesis and determination of their structural properties, in vitro and in vivo performance, *Materials Science and Engineering: C*, 55, pp. 538-546.

[15]   Liu, Y., Hou, D., and Wang, G. (2004). A simple wet chemical synthesis and characterization of hydroxyapatite nanorods, *Materials Chemistry and Physics*, 86, pp. 69-73.

[16]   Nielsen, S.P. (2004). The biological role of strontium, *Bone*, 35, pp. 583-588.

[17]   Tite, T., Popa, A.-C., Balescu, L.M., Bogdan, I.M., Pasuk, I., Ferreira, J.M., and Stan, G.E. (2018). Cationic substitutions in hydroxyapatite: Current status of the derived biofunctional effects and their in vitro interrogation methods, *Materials*, 11, 2081, pp. 1-62.

[18]   Pham, V.-H., Van, H.N., Tam, P.D., and Ha, H.N.T. (2016). A novel 1540 nm light emission from erbium doped hydroxyapatite/β-tricalcium phosphate through co-precipition method, *Materials Letters*, 167, pp. 145-147.

[19]   Donglu, S., (2005). *Introduction to biomaterials*, World Scientific, 1, pp. 3-12.

[20]   Migonney, V. (2014). History of biomaterials, *Biomaterials*, 1, pp. 1-10.

[21]   Park, J. and Lakes, R.S., (2007). *Biomaterials: an introduction*, Springer Science & Business Media, 1(3), pp. 2-9.

[22]   Dean, M.N., Swanson, B.O., and Summers, A.P. (2009). Biomaterials: Properties, variation and evolution, *Integrative and comparative biology*, 49, pp.15-20.

[23]   Mozafari, M. (2014). Bioceramics in the Realm of History, *Bioceramics Dev. Appl.*, 4, e106, pp. 1-2.

[24]   Burdick, J.A. and Mauck, R.L., (2010). *Biomaterials for tissue engineering applications: a review of the past and future trends*, Springer Science & Business Media wein New york, pp. 119-139.

[25]   Von Recum, A.F. and Laberge, M. (1995). Educational goals for biomaterials science and engineering: prospective view, *Journal of applied biomaterials*, 6, pp. 137-144.

[26]   Patel, N.R. and Gohil, P.P. (2012). A review on biomaterials: scope, applications & human anatomy significance, *International Journal of Emerging Technology and Advanced Engineering*, 2, pp. 91-101.

[27]   Rogero, S.O., Malmonge, S.M., Lugão, A.B., Ikeda, T.I., Miyamaru, L., and Cruz, Á.S. (2003). Biocompatibility study of polymeric biomaterials, *Artificial organs*, 27, pp. 424-427.

[28]   Huang, L.L., Sung, H.W., Tsai, C.C., and Huang, D.M. (1998). Biocompatibility study of a biological tissue fixed with a naturally occurring crosslinking reagent, *Journal of Biomedical Materials Research: An Official Journal of The Society for Biomaterials, The Japanese Society for Biomaterials, and The Australian Society for Biomaterials*, 42, pp. 568-576.

[29]   Shabalovskaya, S.A. (2002). Surface, corrosion and biocompatibility aspects of Nitinol as an implant material, *Bio-medical materials and engineering*, 12, pp. 69-109.

[30]   Sathishkumar, S., Karthika, A., Surendiran, M., Kavitha, L., and Gopi, D. (2015). Electrodeposition of cerium substituted hydroxyapatite coating on passivated surgical grade stainless steel for biomedical application, *Int. J. ChemTech. Res.*, 7, pp. 533-538.

[31]   Boutrand, J.-P. Biocompatibility and Performance of Medical Devices. Cambridge, UK: Woodhead Publishing. 2012, *International Journal of Toxicology*, 32, pp. 308e-312e.

[32]   Amato, S.F. and Ezzell Jr, R.M., (2014). *Regulatory affairs for biomaterials and medical devices*, Elsevier, 79, pp. 1-9

[33]   June, W., (1993). *An Introduction To Bioceramics*, World Scientific, 1, pp.1-25.

[34]   Hench, L.L (1999). *Bioactive glasses and glass-ceramics*. in *Materials science forum*, 293, pp. 37-64.

[35]   Hench, L.L. (1991). Bioceramics: from concept to clinic, *Journal of the american ceramic society*, 74, pp. 1487-1510.

[36]   Kaygili, O., Dorozhkin, S.V., Keser, S., and Yakuphanoglu, F. (2015). Investigation of the crystal structure, dielectrical, electrical and microstructural properties of cobalt-containing calcium orthophosphates, *Materials Science*, 21, pp.282-287.

[37]   Heness, G. and Ben-Nissan, B (2004). *Innovative bioceramics*. in *Materials forum*, 27, pp. 104-114.

[38]   Hench, L.L. and Polak, J.M. (2002). Third-generation biomedical materials, *Science*, 295, pp. 1014-1017.

[39] Deville, S., Chevalier, J., Fantozzi, G., Bartolomé, J.F., Requena, J.n., Moya, J.S., Torrecillas, R., and Díaz, L.A. (2003). Low-temperature ageing of zirconia-toughened alumina ceramics and its implication in biomedical implants, *Journal of the European Ceramic Society*, 23, pp. 2975-2982.

[40] Ibrahim, M.Z., Sarhan, A.A., Yusuf, F., and Hamdi, M. (2017). Biomedical materials and techniques to improve the tribological, mechanical and biomedical properties of orthopedic implants–A review article, *Journal of Alloys and Compounds*, 714, pp. 636-667.

[41] Hench, L.L. (1988). Bioactive ceramics, *Annals of the New York academy of sciences*, 523, pp. 54-71.

[42] Daculsi, G., LeGeros, R., Heughebaert, M., and Barbieux, I. (1990). Formation of carbonate-apatite crystals after implantation of calcium phosphate ceramics, *Calcified Tissue International*, 46, pp. 20-27.

[43] Salinas, A.J. and Vallet-Regí, M. (2013). Bioactive ceramics: from bone grafts to tissue engineering, *RSC Advances*, 3, pp. 11116-11131.

[44] Kim, H.-M. (2001). Bioactive Ceramics, *Journal of the ceramic society of Japan*, 109, pp. S49-S57.

[45] Buchanan, F.J., (2008). *Degradation rate of bioresorbable materials: prediction and evaluation*, Elsevier,

[46] Kaygili, O., Keser, S., Ates, T., and Yakuphanoglu, F. (2013). Synthesis and characterization of lithium calcium phosphate ceramics, *Ceramics International*, 39, pp. 7779-7785.

[47] Wang, L. and Nancollas, G.H. (2008). Calcium orthophosphates: crystallization and dissolution, *Chemical reviews*, 108, pp. 4628-4669.

[48] Dorozhkin, S.V. (2010). Bioceramics of calcium orthophosphates, *Biomaterials*, 31, pp. 1465-1485.

[49] de Groot, K. (1993). Clinical applications of calcium phosphate biomaterials: a review, *Ceramics International*, 19, pp. 363-366.

[50] de Groot, K., (2018). *Bioceramics Calcium Phosphate:* CRC press, Florida, pp.5-17.

[51] Bohner, M. (2000). Calcium orthophosphates in medicine: from ceramics to calcium phosphate cements, *Injury*, 31, pp. D37-D47.

[52] Dorozhkin, S.V. and Epple, M. (2002). Biological and medical significance of calcium phosphates, *Angewandte Chemie International Edition*, 41, pp. 3130-3146.

[53] Kaygili, O., Dorozhkin, S.V., Ates, T., Gursoy, N.C., Keser, S., Yakuphanoglu, F., and Selçuk, A.B. (2015). Structural and dielectric properties of yttrium-substituted hydroxyapatites, *Materials Science and Engineering: C*, 47, pp. 333-338.

[54] Zhou, H. and Lee, J. (2011). Nanoscale hydroxyapatite particles for bone tissue engineering, *Acta Biomaterialia*, 7, pp. 2769-2781.

[55] Leventouri, T. (2006). Synthetic and biological hydroxyapatites: crystal structure questions, *Biomaterials*, 27, pp. 3339-3342.

[56] Kattimani, V.S., Kondaka, S., and Lingamaneni, K.P. (2016). Hydroxyapatite––Past, present, and future in bone regeneration, *Bone and Tissue Regeneration Insights*, 7, S 36138, pp. 9-19.

[57] Rodriguez-Lorenzo, L., Vallet-Regí, M., Ferreira, J., Ginebra, M., Aparicio, C., and Planell, J. (2002). Hydroxyapatite ceramic bodies with tailored mechanical properties for different applications, *Journal of biomedical materials research*, 60, pp. 159-166.

[58] Coelho, T., Nogueira, E., Weinand, W., Lima, W., Steimacher, A., Medina, A., Baesso, M., and Bento, A. (2007). Thermal properties of natural nanostructured hydroxyapatite extracted from fish bone waste, *Journal of applied physics*, 101, pp. 084701-1– 084701-6.

[59] De Lange, G. and Donath, K. (1989). Interface between bone tissue and implants of solid hydroxyapatite or hydroxyapatite-coated titanium implants, *Biomaterials*, C 10, 121-125.

[60] Hing, K., Best, S., Tanner, K., Bonfield, W., and Revell, P. (1999). Quantification of bone ingrowth within bone-derived porous hydroxyapatite implants of varying density, *Journal of Materials Science: Materials in Medicine*, 10, pp. 663-670.

[61] Asri, R., Harun, W., Hassan, M., Ghani, S., and Buyong, Z. (2016). A review of hydroxyapatite-based coating techniques: Sol–gel and electrochemical depositions on biocompatible metals, *Journal of the mechanical behavior of biomedical materials*, 57, pp. 95-108.

[62] Cacciotti, I. (2014). Cationic and anionic substitutions in hydroxyapatite, *Handbook of bioceramics and biocomposites*, C, pp. 1-68.

[63] Šupová, M. (2015). Substituted hydroxyapatites for biomedical applications: a review, *Ceramics International*, 41, pp. 9203-9231.

[64] Curran, D.J., Fleming, T.J., Towler, M.R., and Hampshire, S. (2011). Mechanical parameters of strontium doped hydroxyapatite sintered using microwave and conventional methods, *Journal of the mechanical behavior of biomedical materials*, 4, pp. 2063-2073.

[65] Neacsu, I.A., Stoica, A.E., Vasile, B.S., and Andronescu, E. (2019). Luminescent hydroxyapatite doped with rare earth elements for biomedical applications, *Nanomaterials*, 9(239). pp. 1-21.

[66] De Araujo, T., De Souza, S., and De Sousa, E (2010). *Effect of Zn2+, Fe3+ and Cr3+ addition to hydroxyapatite for its application as an active constituent of sunscreens*. in *Journal of Physics: Conference Series*, 249, pp. 1-8

[67] Ravindranadh, K., Babu, B., Manjari, V.P., Rao, G.T., Rao, M., and Ravikumar, R. (2015). Optical and structural properties of undoped and Mn2+ doped Ca–Li hydroxyapatite nanopowders using mechanochemical synthesis, *Journal of Luminescence*, 159, pp. 119-127.

[68] Alshemary, A.Z., Akram, M., Goh, Y.-F., Kadir, M.R.A., Abdolahi, A., and Hussain, R. (2015). Structural characterization, optical properties and in vitro bioactivity of mesoporous erbium-doped hydroxyapatite, *Journal of Alloys and Compounds*, 645, pp. 478-486.

[69] Cullity, D. Elements of X–Ray diffraction" libro, *Addison–Wesley Publishing Company*, 2, pp. 81-106.

[70] Kaygili, O. and Keser, S. (2016). Zr/Mg, Zr/Sr and Zr/Zn co-doped hydroxyapatites: synthesis and characterization, *Ceramics International*, 42, pp. 9270-9273.

[71] Yogamalar, R., Srinivasan, R., Vinu, A., Ariga, K., and Bose, A.C. (2009). X-ray peak broadening analysis in ZnO nanoparticles, *Solid State Communications*, 149, pp. 1919-1923.

[72] Mansour, S., El-Dek, S., Dorozhkin, S., and Ahmed, M. (2017). Physico-mechanical properties of Mg and Ag doped hydroxyapatite/chitosan biocomposites, *New Journal of Chemistry*, 41, pp.13773-13783.

[73] Mote, V., Purushotham, Y., and Dole, B. (2012). Williamson-Hall analysis in estimation of lattice strain in nanometer-sized ZnO particles, *Journal of Theoretical and Applied Physics*, 6 (6). pp. 1-8.

[74] Landi, E., Tampieri, A., Celotti, G., and Sprio, S. (2000). Densification behaviour and mechanisms of synthetic hydroxyapatites, *Journal of the European Ceramic Society*, 20, pp. 2377-2387.

[75] Yasukawa, A., Gotoh, K., Tanaka, H., and Kandori, K. (2012). Preparation and structure of calcium hydroxyapatite substituted with light rare earth ions, *Colloids and Surfaces A: Physicochemical and Engineering Aspects*, 393, pp. 53-59.

[76] Jesser, W. and Kuhlmann-Wilsdorf, D. (1967). On the theory of interfacial energy and elastic strain of epitaxial overgrowths in parallel alignment on single crystal substrates, *physica status solidi (b)*, 19, pp. 95-105.

[77] Gamal, G., Al-Mufadi, F., and Said, A. (2013). Effect of iron additives on the microstructure of hydroxyapatite, *Engineering, Technology & Applied Science Research*, 3, pp. 532-539.

[78] Moghaddam, H.M. and Nasirian, S. (2012). Dependence of activation energy and lattice strain on TiO 2 nanoparticles?, *Nanoscience Methods*, 1, pp. 201-212.

[79] Venkateswarlu, K., Bose, A.C., and Rameshbabu, N. (2010). X-ray peak broadening studies of nanocrystalline hydroxyapatite by Williamson–Hall analysis, *Physica B: Condensed Matter*, 405, pp. 4256-4261.

[80] Xu, G., Aksay, I.A., and Groves, J.T. (2001). Continuous crystalline carbonate apatite thin films. A biomimetic approach, *Journal of the American Chemical Society*, 123, pp. 2196-2203.

[81] Raynaud, S., Champion, E., Bernache-Assollant, D., and Thomas, P. (2002). Calcium phosphate apatites with variable Ca/P atomic ratio I. Synthesis, characterisation and thermal stability of powders, *Biomaterials*, 23, pp. 1065-1072.

[82] Giannozzi, P., Baroni, S., Bonini, N., Calandra, M., Car, R., Cavazzoni, C., Ceresoli, D., Chiarotti, G.L., Cococcioni, M., and Dabo, I. (2009). QUANTUM ESPRESSO: a modular and open-source software project for quantum simulations of materials, *Journal of Physics: Condensed Matter*, 21, 395502, pp. 1-17.

[83] Avakyan, L.A., Paramonova, E.V., Coutinho, J., Öberg, S., Bystrov, V.S., and Bugaev, L.A. (2018). Optoelectronics and defect levels in hydroxyapatite by first-principles, *The Journal of chemical physics*, 148, pp. 154706-1–154706-2.

[84] Slepko, A. and Demkov, A.A. (2011). First-principles study of the biomineral hydroxyapatite, *Physical Review B*, 84, pp. 134108-1–134108-11..

[85] Azzouz, L., Halit, M., Charifi, Z., and Matta, C.r.F. (2019). Tellurium Doping and the Structural, Electronic, and Optical Properties of NaYS2 (1–x) Te2 x Alloys, *ACS omega*, 4, pp. 11320-11331.

CURRICULUM VITAE

Bahroz Kareem MAHMOOD

PERSONAL INFORMATIONS

Birth of Place	**:** Shahrazoor/ Sulaimani
Birth of Date	**:** 1990
Nationality	**:** Iraq
Address	**:** University of Sulaimani
E-mail	**:** Bahroz.K.mahmood@gmail.com
Languages	**:** Turkish (C1), English (B2)

EDUCATION

Bachelor	**:** University of Sulaimani, College of Education, Physics Department, 2011
High School	**:** Shahed Sarchl Preparatory for Boys, Sulaimani

ACADEMIC ACTIVITIES

Paper:

1. Mahmood, B.K., Kaygili, O., Bulut, N., Dorozhkin, S.V., Ates, T., Koytepe, S., Gürses, C., Ercan, F., Kebiroglu, H., Agid, R.S. and İnce, T. (2020). Effects of strontium - erbium co-doping on the structural properties of hydroxyapatite: an experimental and theoretical study, *Ceramics International*, 46, pp. 16354-16363.

Proceedings:

1. Turan İnce, Hanifi Kebiroglu, Tankut Ates, Fatih Firdolas, Bahroz Kareem Mahmood, Serhat Keser, Niyazi Bulut, Omer Kaygili (2019), Determination of Dielectric Properties of Calcium Orthophosphates, 2nd International Conference on Physical Chemistry and Functional Materials (PCFM'19), Oral Presentation, p. 28, June 25-27, Cappadocia, Turkey.

2. Bahroz Kareem Mahmood, Tankut Ates, Hanifi Kebiroglu, Fatih Firdolas, Turan İnce, Serhat Keser, Omer Kaygili, Niyazi Bulut (2019), An X-Ray Diffraction Study of Mg/Fe Co-Doped Biphasic Calcium Phosphates, 2nd International Conference on Physical Chemistry and Functional Materials (PCFM'19), Oral Presentation, p. 115, June 25-27, Cappadocia, Turkey.

3. Bahroz Kareem Mahmood, Havva Esma Okur, Tankut Ates, Hanifi Kebiroglu, Fatih Firdolas, Turan İnce, Serhat Keser, Omer Kaygili, Niyazi Bulut (2019), Williamson-Hall Analysis of Sm-Doped ZnO Samples, 2nd International Conference on Physical Chemistry and Functional Materials (PCFM'19), p. 36, June 25-27, Cappadocia, Turkey.

4. Tankut Ates, Hanifi Kebiroglu, Turan İnce, Fatih Firdolas, Bahroz Kareem Mahmood, Omer Kaygili, Serhat Keser, Niyazi Bulut (2019), X-Ray Diffraction Analysis of Ni-

Doped Zinc Aluminates, 2nd International Conference on Physical Chemistry and Functional Materials (PCFM'19), p. 38, June 25-27, Cappadocia, Turkey.

5. Turan İnce, Serdar Acar, Ibrahim Isah Nasidi, Hanifi Kebiroglu, Bahroz Kareem Mahmood, Riyadh Saeed Agid, Lale Ibrahimzade, Tankut Ates, Niyazi Bulut, Omer Kaygili (2019), An X-Ray Diffraction Study of Mn-doped Hydroxyapatite, Oral Presentation, Anadolu Kongreleri 3. Uluslararası Uygulamalı Bilimler Kongresi, pp. 401-402, 28-29 December, Diyarbakır, Turkey.

6. Turan İnce, Serdar Acar, Ibrahim Isah Nasidi, Hanifi Kebiroglu, Bahroz Kareem Mahmood, Riyadh Saeed Agid, Lale Ibrahimzade, Tankut Ates, Niyazi Bulut, Omer Kaygili (2019), A Theoretical Study on Acetophenone Molecule, Oral Presentation, Anadolu Kongreleri 3. Uluslararası Uygulamalı Bilimler Kongresi, pp. 399-400, 28-29 December, Diyarbakır, Turkey.

7. Hanifi Kebiroglu, Lala Ibrahimzade, Bahroz Kareem Mahmood, Serdar Acar, Turan Ince, Ibrahim Isah Nasidi, Niyazi Bulut, Omer Kaygili (2020), Combustion Synthesis and Morphological Investigation of CuO, IV. Uluslararası Battalgazi Bilimsel Çalışmalar Kongresi, p.46, 29 February- 1 March, Malatya, Turkey.

8. Hanifi Kebiroglu, Bahroz Kareem Mahmood, Serdar Acar, Turan Ince, Lala Ibrahimzade, Ibrahim Isah Nasidi, Niyazi Bulut, Omer Kaygili (2020), Investigation of Band Structures of Yttrium-Doped Hydroxyapatites, IV. Uluslararası Battalgazi Bilimsel Çalışmalar Kongresi, p.45, 29 February- 1 March, Malatya, Turkey.

9. Bahroz Kareem Mahmood, Serdar Acar, Turan Ince, Hanifi Kebiroglu, Ibrahim Isah Nasidi, Niyazi Bulut, Omer Kaygili (2020), A Potential Surface Energy (PES) Analysis of Benzonitrile Molecule, 3. Uluslararası Mardin Artuklu Bilimsel Araştırmalar Kongresi, pp. 178-179, 18-19 January, Mardin, Turkey.

10. Lala Ibrahimzade, Bahroz Kareem Mahmood, Serdar Acar, Turan Ince, Hanifi Kebiroglu, Ibrahim Isah Nasidi, Niyazi Bulut, Omer Kaygili (2020), A Theoretical Calculation of the Bandgap Energies of Ag-Doped Hydroxyapatites, 3. Uluslararası Mardin Artuklu Bilimsel Araştırmalar Kongresi, p. 175, 18-19 January, Mardin, Turkey.